Mathematisch-Naturwissenschaftliche Fakultät
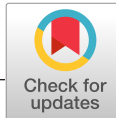
Alessia Borghini | Silvio Ferrero | Patrick J. O'Brien | Oscar Laurent |
Christina Günter | Martin A. Ziemann

Cryptic metasomatic agent measured in situ in Variscan mantle rocks

Melt inclusions in garnet of eclogite, Granulitgebirge, Germany

ORIGINAL ARTICLE

Cryptic metasomatic agent measured in situ in Variscan mantle rocks: Melt inclusions in garnet of eclogite, Granulitgebirge, Germany

Alessia Borghini[1] | Silvio Ferrero[1,2] | Patrick J. O'Brien[1] | Oscar Laurent[3] |
Christina Günter[1] | Martin A. Ziemann[1]

[1]Institut für Geowissenschaften, Universität Potsdam, Potsdam, Germany

[2]Museum für Naturkunde (MfN), Leibniz-Institut für Evolutions- und Biodiversitätsforschung, Berlin, Germany

[3]Eidgenössische Technische Hochschule, ETH, Zürich, Switzerland

Correspondence
Alessia Borghini, Institut für Geowissenschaften, Universität Potsdam, Potsdam, Germany.
Email: borghini@uni-potsdam.de

Funding information
Deutsche Forschungsgemeinschaft, Grant/Award Number: FE 1527/2-1 and FE 1527/2-2

Handling Editor: Bernardo Cesare

Abstract

Garnet of eclogite (formerly termed garnet clinopyroxenite) hosted in lenses of orogenic garnet peridotite from the Granulitgebirge, NW Bohemian Massif, contains unique inclusions of granitic melt, now either glassy or crystallized. Analysed glasses and re-homogenized inclusions are hydrous, peraluminous, and enriched in highly incompatible elements characteristic of the continental crust such as Cs, Li, B, Pb, Rb, Th, and U. The original melt thus represents a pristine, chemically evolved metasomatic agent, which infiltrated the mantle via deep continental subduction during the Variscan orogeny. The bulk chemical composition of the studied eclogites is similar to that of Fe-rich basalt and the enrichment in LILE and U suggest a subduction-related component. All these geochemical features confirm metasomatism. In comparison with many other garnet+clinopyroxene-bearing lenses in peridotites of the Bohemian Massif, the studied samples from Rubinberg and Klatschmühle are more akin to eclogite than pyroxenites, as reflected in high jadeite content in clinopyroxene, relatively low Mg, Cr, and Ni but relatively high Ti. However, trace elements of both bulk rock and individual mineral phases show also important differences making these samples rather unique. Metasomatism involving a melt requiring a trace element pattern very similar to the composition reported here has been suggested for the source region of rocks of the so-called durbachite suite, that is, ultrapotassic melanosyenites, which are found throughout the high-grade Variscan basement. Moreover, the Th, U, Pb, Nb, Ta, and Ti patterns of these newly studied melt inclusions (MI) strongly resemble those observed for peridotite and its enclosed pyroxenite from the T-7 borehole (Staré, České Středhoři Mountains) in N Bohemia. This suggests that a similar kind of crustal-derived melt also occurred here. This study of granitic MI in eclogites from peridotites has provided the first direct characterization of a preserved metasomatic melt, possibly responsible for the metasomatism of several parts of the mantle in the Variscides.

KEYWORDS

clinopyroxenite, eclogite, melt inclusions, metasomatism, orogenic peridotite

1 | INTRODUCTION

Orogenic peridotites are ultrabasic bodies tectonically emplaced in suture zones and mountain belts (Bodinier & Godard, 2014). These bodies have attracted the attention of the scientific community because they offer a potential source of information on mantle processes, such as the transport, reaction, and storage of melts and/or fluids in supra-subduction mantle wedges, as well as on subduction/exhumation mechanisms (Allègre & Turcotte, 1986; Bodinier & Godard, 2014 and references therein; Brueckner, 1998). The upper mantle has been shown to be chemically heterogeneous and it is common to find veins, dykes, and lenses of websterite, pyroxenite, and eclogite in exposed peridotites (Becker, 1996; Bodinier & Godard, 2014; Borghini et al., 2018; Brueckner & Medaris, 2000; Garrido & Bodinier, 1999; Medaris et al., 1995; Svojtka et al., 2016).

Despite decades of research, the origin of pyroxenite and eclogite in orogenic peridotite is still debated although most theories involve a melt component and oceanic (±continental) crust. The predominant hypothesis is a high pressure (HP) cumulate origin of garnet and clinopyroxene (Bodinier & Godard, 2014; Bodinier, Guiraud, Fabriès, Dostal, & Dupuy, 1987; Garrido & Bodinier, 1999; Svojtka et al., 2016) from basaltic melts deriving from either the asthenospheric mantle (Becker, 1996; Schmädicke, Gose, & Will, 2010) or mantle metasomatized by melting of subducted oceanic crust (Medaris et al., 1995; Medaris, Wang, Jelínek, Mihaljevič, & Jakeš, 2005; Schmädicke et al., 2010). Another possibility proposed is a metasomatic interaction between a melt and the mantle peridotite at the margin of a melt conduit (Malaspina, Hermann, & Scambelluri, 2009; Malaspina, Hermann, Scambelluri, & Compagnoni, 2006; Vrijmoed et al., 2013). Some garnet clinopyroxenites are interpreted as HP recrystallized variants of layers originating as basalts/gabbros (e.g. Obata, Hirajima, & Svojtka, 2006; Svojtka et al., 2016). These are mostly eclogites but varieties with low-Na clinopyroxene also exist. Moreover, also stress-induced recrystallization of high temperature (HT; 1,300–1,400°C) highly aluminous pyroxene megacrysts can generate, typically at HP and lower temperatures, exsolution-like lamellar garnet and low-Al pyroxene growth (Carswell & Jamtveit, 1990; Faryad, Dolejš, & Machek, 2009; Massonne & Bautsch, 2002; Medaris et al., 2005; Schmädicke et al., 2010). The megacrysts originally formed from interaction between the mantle and mantle-derived melts, which produced mono-mineralic layers of clinopyroxene and/or orthopyroxene and/or garnet (Massonne & Bautsch, 2002; Schmädicke et al., 2010). A full understanding of the formation of pyroxenite and eclogite would thus provide new insights on melt-related processes in mafic and ultramafic rocks and on the nature of crust–mantle interactions in a variety of subduction settings. Typically,

investigation of the evolution of these rocks is via trace element and isotope studies. However, the most direct approach to study any deep process involving fluids is clearly to investigate the fluid/melt itself, such as when it is preserved as primary inclusions, thus revealing crucial information about the genesis of both fluid/melt and its host phase (Ferrero & Angel, 2018).

Two localities in the Granulitgebirge (northern part of the Bohemian Massif), Rubinberg and Klatschmühle, show the occurrence of eclogite (formerly termed garnet clinopyroxenite) lenses in orogenic peridotite that is itself enclosed in HP felsic granulite. Primary melt inclusions (MI) were already reported in these eclogites and the melt was interpreted as having been directly involved in their formation (Borghini et al., 2018). Although these eclogites were already reported in studies on orogenic peridotites and granulites of the Granulitgebirge (Rötzler, Hagen, & Hoernes, 2008; Schmädicke et al., 2010), no detailed geochemical and microstructural investigation was ever undertaken, and the presence of preserved MI went unnoticed until the work of Borghini et al. (2018). The present paper contains the first detailed geochemical data set on these so far unique melt-bearing garnet+clinopyroxene-rich rocks, and includes analyses of the bulk rock, the main mineral phases, and the trapped melt. The aim is to compare this newly acquired geochemical data set with published data for similar rocks from other localities in the Bohemian Massif in order to define the role of deep melts in the metasomatic interaction between the crust and the mantle during continental subduction.

2 | GEOLOGICAL SETTING

The European Variscides are part of an 8,000 km long orogenic belt generated after the collision of Laurasia and Gondwana during the late Palaeozoic era (O'Brien, 2000; O'Brien & Carswell, 1993) and exposed in a series of uplifted basement blocks such as the Iberian, Armorican, and Bohemian Massifs and the French Massif Central. At the easternmost part of the chain, the Bohemian Massif, high-grade crystalline rocks extend into parts of Germany, the Czech Republic, Poland, and Austria (O'Brien & Carswell, 1993; Figure 1). The Variscan evolution of this basement can be divided into a Devonian oceanic subduction followed by Devonian–Carboniferous deep continental subduction and continental collision, which resulted in high-grade metamorphism at different pressures and widespread late intrusion of granitoids (Franke, 2000; O'Brien, 2000; Schulmann, Lexa, Janoušek, Lardeaux, & Edel, 2014; Scott, Konrad-Schmolke, O'Brien, & Günter, 2013; Timmerman, 2008). Traditionally, the high-grade part of the Variscan core is called the Moldanubian Zone, whereas a mostly lower grade region to the north is called the Saxothuringian Zone. However,
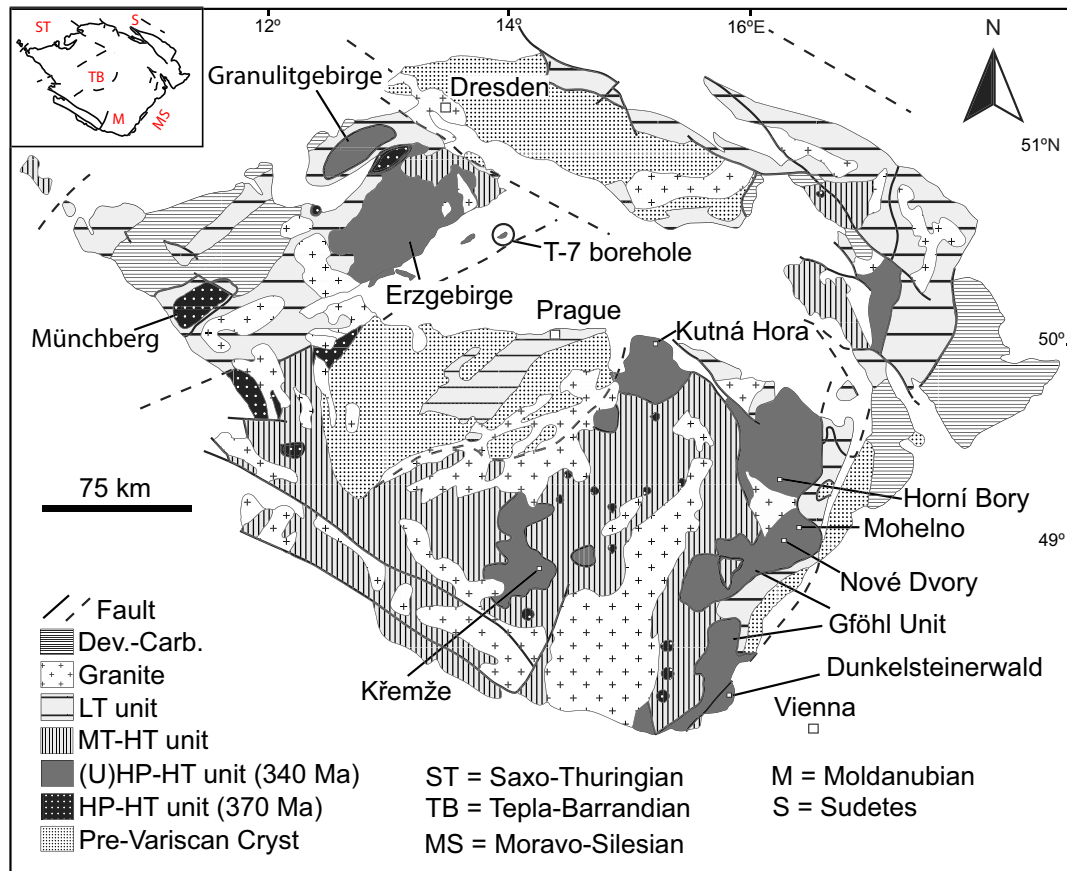
FIGURE 1 Simplified geological map of the Bohemian Massif (modified after Franke & Żelaźniewicz, 2000). The inset reports the different tectonic domains in which the Bohemian Massif is divided

high-grade eclogite, granulite, and peridotite—including diamond- (Kotková, O'Brien, & Ziemann, 2011; Nasdala & Massonne, 2000) and coesite-bearing rocks (Kotková et al., 2011; Massonne, 2001)—are located in both of these zones, questioning this traditional subdivision (Franke, 1989; Matte, Maluski, Rajlich, & Franke, 1990; Medaris et al., 1995; O'Brien & Carswell, 1993).

For the most part, older (380–400 Ma) eclogites are associated with spinel peridotites, whereas younger, 340 Ma eclogites and so-called HP granulites (eclogite facies metagranitic rocks) occur with serpentinized garnet peridotites. Such garnet peridotite bodies are reported mainly from five different granulite terrains in the Bohemian Massif: the Saxonian Granulite Complex (Granulitgebirge, Saxothuringian Zone), the Ohře Crystalline complex and České Středohoři Mountains (Saxothuringian Zone, NW of Prague), Sowie Góry (Sudetes, Poland), the Gföhl Unit in South Bohemia, Lower Austria and West Moravia (Medaris & Carswell, 1990). The host rocks in all cases are felsic HP granulites (eclogite facies metagranites with granulite facies overprint; O'Brien & Rötzler, 2003) or their migmatized version, termed Gföhl gneiss (Cooke & O'Brien, 2001).

This study focusses on the Saxonian Granulite complex in the Granulitgebirge.

The Granulitgebirge, well known for the granulite type locality (Weiss, 1803), is located on the northwestern portion of the Saxothuringian Zone (eastern Germany) (Figures 1 and 2). It comprises a NE–SW trending dome-like body over 50 km long and 20 km wide mostly made of HP quartzofeldspathic granulites with minor layers of pyroxene-bearing granulites of intermediate to basic composition, which represent the deepest structural unit (Carswell & O'Brien, 1993; O'Brien, 2000; O'Brien, 2006, 2008; O'Brien & Rötzler, 2003; Rötzler et al., 2008; Schmädicke et al., 2010). A detachment fault divides the granulite from the lowest structural unit of the Schist Cover. These schists experienced a low-P HT metamorphism related to the emplacement of the hot granulites via 'hot core complex' extensional mechanism (O'Brien & Carswell, 1993; Reinhardt & Kleemann, 1994). Between these two structural units, slivers of cordierite- and garnet-rich gneisses, metaophiolites, and orthogneisses may occur. All this complex is then intruded by stocks and sills of monzogranite (O'Brien, 2000; Rötzler et al., 2008; Schmädicke et al., 2010 and references therein; Figure 2).

The dominant lithology in the Granulitgebirge consists of granulite with hypersolvus ternary feldspar (now mesoperthite) and quartz with a variable amount of garnet and kyanite
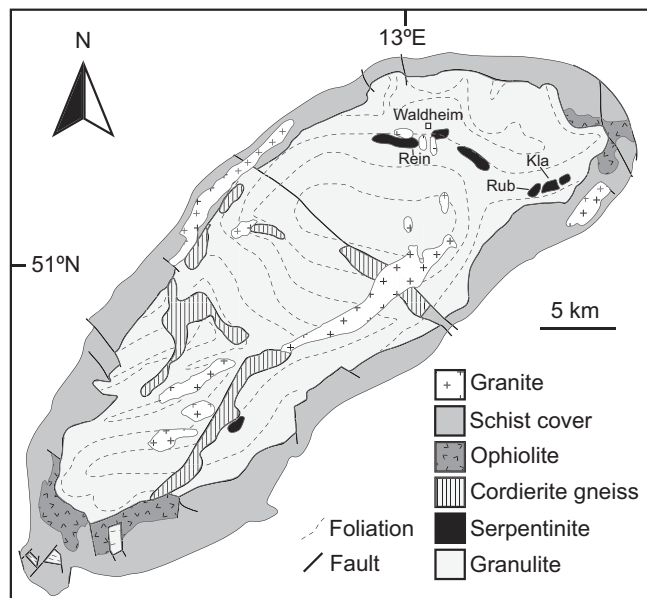
FIGURE 2 Schematic geological map of the Granulitgebirge (modified after Rötzler et al., 2008) with locations of the two selected areas, Rub = Rubinberg and Kla = Klatschmühle, and the localities with the former clinopyroxene megacrysts (see text for details). Rein = Reinsdorf

along with rutile, apatite, and zircon as accessories (O'Brien, 2006, 2008; Rötzler & Romer, 2001). Granulites have a mylonitic structure with platy quartz and sometimes a banding defined by secondary biotite (O'Brien, 2006, 2008; Rötzler et al., 2008). Geochemical and isotope data suggest that most of the granulites have an igneous origin (Rötzler et al., 2008; Werner, 1987) with a protolith age *c.* 470–485 Ma (Kröner, Jaeckel, Reischmann, & Kroner, 1998; Romer & Rötzler, 2001; Rötzler, Romer, Budzinski, & Oberhänsli, 2004; von Quadt, 1993). Enclosed in the felsic rocks are bodies of serpentinized garnet peridotite, which in turn contain layers and lenses of garnet+clinopyroxene-rich rocks (Borghini et al., 2018; Massonne & Bautsch, 2002; O'Brien & Carswell, 1993; O'Brien, 2008; Rötzler et al., 2008; Schmädicke et al., 2010).

The *P*-temperature (*T*) peak conditions estimated for the granulite and garnet clinopyroxenite are 1,000–1,015°C and 2.0–2.2 GPa (Rötzler et al., 2008), ultra-HT eclogitic facies, and the metamorphic peak at *c.* 340 Ma (Rötzler & Romer, 2001) was followed by rapid exhumation and cooling to middle crustal levels (O'Brien & Rötzler, 2003). Similar metamorphic ages are observed in comparable felsic granulite–peridotite–pyroxenite complex rocks elsewhere in the high-grade Variscan core, for example, in the Erzgebirge, North Bohemia and Gföhl unit of the Moldanubian Zone, thus suggesting a common early evolution. However, the age determined for the pyroxenite of Klatschmühle is instead 380 Ma (von Quadt, 1993) and this aspect will be discussed below (Section 6.1).

3 | METHODS AND SAMPLE SELECTION

The study has been performed on ~30 μm thin- and double-polished thick sections (150 μm thick). Sample preparation, petrographic study with a polarized light optical microscope, micro-Raman and electron microprobe (EMP) analysis were performed at the Institut für Geowissenschaften of the University of Potsdam. The micro-Raman analyses were carried out using a HORIBA Jobin Yvon Confocal LabRAM HR 800 equipped with a Peltier-cooled multichannel CCD detector and an Olympus BX41 petrographic microscope. The excitation was obtained using an air-cooled Nd:YAG laser ($\lambda = 532$ nm, laser power on the sample was 2–3 mW) with the 100× objective. The slit width was set to 100 μm and the confocal hole to 200 μm. All the spectra were acquired with a grating of 300 lines/mm using the multiwindows option in the wavenumber range between 100 and 4,000 cm^{-1} integrating three repetitions of 100s with spectral resolution of ~10 cm^{-1} (see procedure in Ferrero, Wunder, Walczak, O'Brien, & Ziemann, 2015). A microprobe JEOL JXA-8200 was used to analyse glass and rock mineral phases. The analyses of re-homogenized glassy inclusions reported in this paper are the same used for Borghini et al. (2018) and they have been acquired with a beam diameter of 1 μm, 15 kV, and 3.5 nA. The microprobe has been calibrated with H_2O-bearing leucogranitic glass standards and the same analytical conditions have been applied in each session. The glass standard with H_2O content similar to the glassy inclusions has been used to estimate the correction factor for Na, K, Al, and Si because of the common alkali loss in the analyses on alkali-rich melt (Morgan & London, 2005). The field emission gun electron microprobe (FEG-EMP) JEOL Hyperprobe JXA-8500F of the Museum für Naturkunde in Berlin was used to acquire backscattered electron images and energy-dispersive spectrometer elemental maps for high-resolution microstructural and microchemical investigation.

The trace element contents were quantified using laser ablation inductively coupled plasma mass spectrometry (LA-ICP-MS) at the Department of Earth Sciences, ETH Zürich. The analyses were performed on one thick section for each locality to study the trace elements of mineral phases and on 21 garnet chips separated from two double-polished thick sections (11 chips for Rubinberg and 10 chips for Klatschmühle) to investigate trace elements in selected, unexposed glassy, and crystallized inclusions. For the analyses of trace elements in minerals, a RESOlution (Australian Scientific Instruments/Applied Spectra) laser ablation system equipped with an S-155 dual-volume ablation cell (Laurin Technic, Australia) with an effective volume of ~1 cm^3 has been used. A laser repetition rate of 5 Hz, on-sample energy density of ~3.5 J/cm^2, and spot size of 29 μm has been used for these analyses. The ETH-prototype GeoLas laser ablation system equipped

with an Excimer ArF (193 nm) COMPex 102F laser source (Coherent, Germany) was used for the MI analyses. A laser repetition rate of 10 Hz, on-sample energy densities in the range of 5–10 J/cm^2, and spot sizes between 10 and 30 μm, based on the different inclusion sizes, were used. In general, the inclusion diameter was slightly smaller than the selected spot size in order to ablate completely the inclusion and avoid the unrepresentative sampling related to heterogeneity therein. This paper reports a limited version of the MI data set of Borghini et al. (2018) with a selection of the inclusions with the strongest signal (i.e. highest signal-to-background ratio).

Both laser systems were coupled with an Element XR (Thermo Fischer, Germany) sector-field ICP-MS. The carrier gas consisted of high-purity He (5.0 grade, 0.5–1.0 L/min), to which was admixed make-up Ar gas (6.0 grade, 0.9–1.0 L/min). For all analyses, the instrument was optimized based on the ablation of the NIST SRM612 glass (43 μm raster at 5 μm/s, 10 Hz, and 3.5 J/cm^2) for highest sensitivity on the high mass range, low production of oxides ($^{248}ThO^+/^{232}Th^+$ <0.4%), and U/Th of ~1. The intensities were acquired in low-resolution, peak jumping, and triple detector mode, with a dwell time of 10 ms for all elements (total sweep times were 750 ms for minerals and 782 ms for MIs). The list of isotopes used for each element is reported in the data repository of Borghini et al. (2018) for the different types of analyses.

The glass reference material NIST SRM610 (Jochum et al., 2011) has been used for drift correction and the quantification of the inclusion analyses, ablated at the same conditions as the unknowns, except for an energy density of ~5 J/cm^2 and spot size of 40 μm for MI analyses (for more details see data repository of Borghini et al., 2018). The USGS glass reference materials, GSD-1G and GSE-1G, were used as validation reference materials (respectively for minerals and MI analyses) to check the accuracy and reproducibility of the analyses. All data processing was performed offline. The acquired time-resolved signals were processed using the software SILLS (Guillong, Meier, Allan, Heinrich, & Yardley, 2008). EMP concentrations were used as internal standards for deconvolution of host and inclusion signals and relative sensitivity correction for both mineral phases and inclusions. The EMP concentration of Al_2O_3 has been used as the internal standard for garnet, whereas CaO has been used for clinopyroxene. For the MI analyses, the EMP concentration of Na_2O in the melt has been used as the internal standard, whereas FeO (for Rubinberg) and MgO (for Klatschmühle) have been used as the matrix-only tracer. The elements more enriched in the host (e.g. Y, HREE) with respect to the inclusions are not quantifiable using this method because of the dominance of the host signal, which prevents the deconvolution software from successfully discriminating and quantifying their concentration in the inclusions.

4 | FIELD OCCURRENCE AND SAMPLE PETROGRAPHY

The investigated garnet+clinopyroxene-rich rocks occur as boudinaged layers surrounded by foliated peridotite at two localities: Rubinberg (RUB; 51°1′57″N, 13°7′37″E) and Klatschmühle (KLA; 51°2′38″N, 13°8′43″E; Figure 2). At RUB, the samples are from an abandoned quarry where one single layer of garnet+clinopyroxene-rich rock, ~25 cm thick and 25 m long, is present, whereas at KLA the outcrop is on a slope and the single layer is 40 cm thick and 5 m long (Figure 3a,b). The host in both cases is a serpentinized garnet peridotite with foliation defined by lozenge-shaped pyroxene in which coarse-grained crystals of garnet (>5 mm in diameter) and fragmented olivine occur as relicts in a matrix dominated by serpentine. The garnet+clinopyroxene-rich layers are oriented parallel to the main foliation in the peridotite and they have sharp contacts with the host.

The garnet+clinopyroxene-rich rocks of the two localities show similar petrographic features (Figure 3c,d). They have a granoblastic texture dominated by slightly variable amounts of garnet (40–45% in volume) and clinopyroxene (45%) constituting the assemblage at the HP-UHT metamorphic peak with rutile and ilmenite as accessories. The matrix is medium- to fine-grained and contains interstitial plagioclase, late brown amphibole—in places associated with ilmenite and apatite (Figure 3f) and rare late biotite. The matrix assemblage represents a post-peak stage in the rock history. Leucocratic pockets (Figure 3e) of fine-grained plagioclase occur in some of the samples and show gradational contact with the host rock. The more retrogressed samples show a larger amount of matrix phases and fresh garnet and clinopyroxene occurring only as relicts.

In the investigated samples garnet is euhedral, 1–2 mm in diameter and colourless. It contains clinopyroxene—sometimes rimmed by plagioclase films—rutile, ilmenite, and MI mainly organized in clusters or in some cases in secondary/pseudosecondary trails (Figure 4). Dark trails of fluid inclusions crossing the whole crystal are often visible. Garnet generally contains cracks filled with plagioclase and green amphibole. Along rims it may be replaced by (a) a symplectite of plagioclase and green amphibole; (b) plagioclase coronas/films; or (c) brown amphibole in fine-grained films or associated with ilmenite and apatite (Figure 3f). Clinopyroxene is generally 1–3 mm long, subhedral, pale beige and it has a short prismatic shape with often a cloudy core and a clear rim. In the core, it can contain plagioclase in lamellae and blebs and rutile inclusions. Along the rim, clinopyroxene is partially replaced by brown amphibole, sometimes in an aggregate of ilmenite with or without apatite.

Plagioclase, more abundant in the retrogressed samples, is mainly interstitial. It can also occur in leucocratic pockets. In the fresh samples it forms more or less continuous thin films around garnet (Figure 3d) and clinopyroxene and it shows
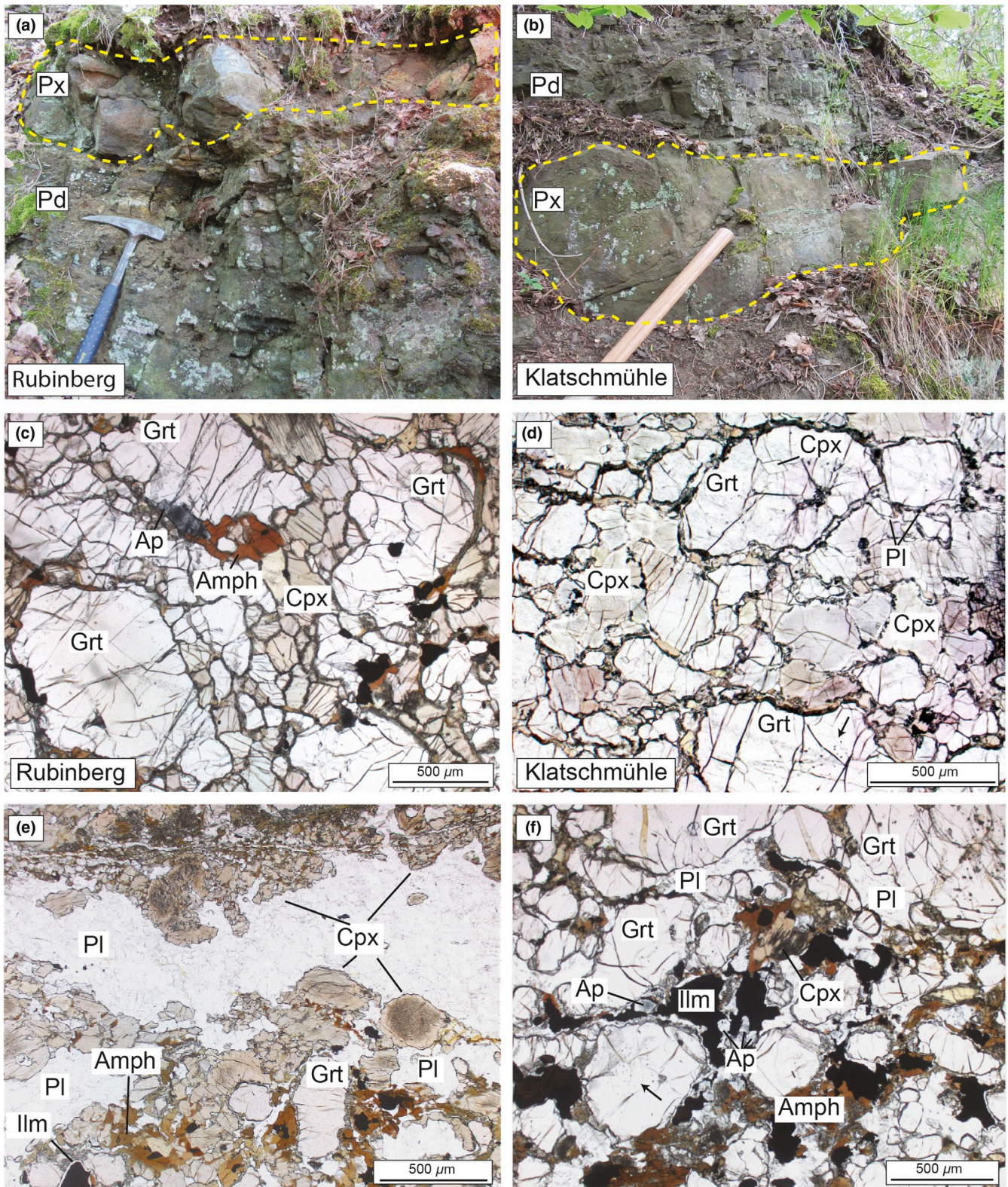
FIGURE 3 Field occurrence of the eclogite, formerly called garnet clinopyroxenite (Px), marked by a yellow dashed line, in Rubinberg (a) and Klatschmühle (b) enclosed in the foliated peridotite (Pd). Plane-polarized photomicrographs of the garnet clinopyroxenites with a granoblastic texture (c, d) dominated by garnet (Grt) and clinopyroxene (Cpx). The matrix contains plagioclase (Pl), both interstitial and in (e) leucocratic pockets, (f) brown amphibole (Amph) in some cases associated with ilmenite (Ilm) and apatite (Ap)
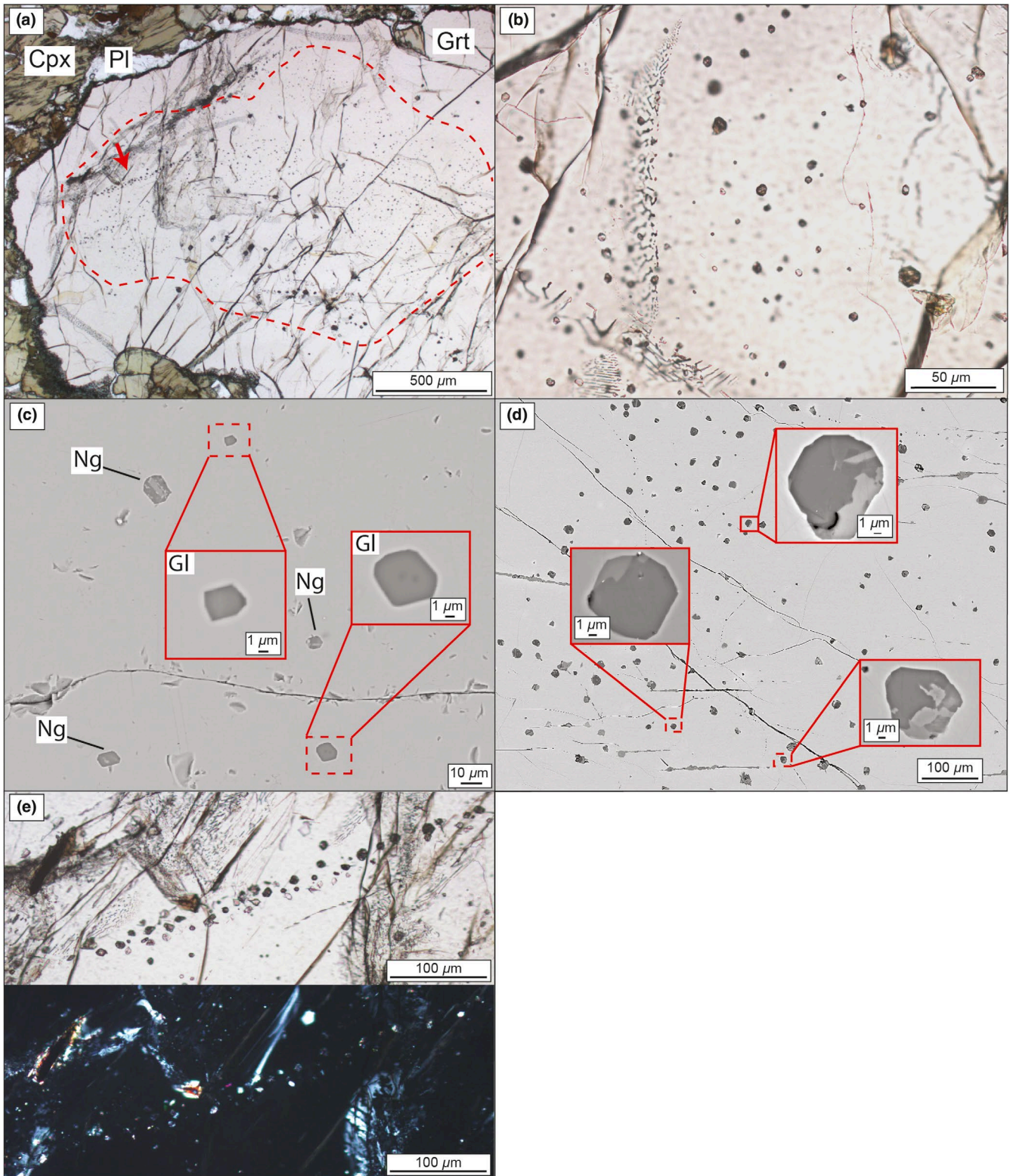
FIGURE 4 Photomicrographs (a, b, e) and backscattered electron (BSE) images (c, d) of the melt inclusion occurrences in both Rubinberg (a–e) and Klatschmühle (b–d) eclogites. (a) Melt inclusion distribution in clusters in the inner part of the garnet (indicated by the dashed red contour) or as trails that cross-cut garnet crystals and the MI cluster (red arrow). (b) Clusters with primary nanogranitoids. (c) Cluster made of nanogranitoids (Ng) and glassy (Gl) inclusions (indicated with dashed red squares). (d) Details of a cluster with nanogranitoids with a well-developed isometric shape. (e) Melt inclusions trail cross-cutting the garnet at parallel (top) and crossed polars (bottom)

polysynthetic twinning. In the leucocratic pockets the plagioclase is fine grained with a patchy extinction and often with subgrain microstructures (Figure 3e). The brown amphibole in the matrix often forms aggregates with ilmenite±apatite and it is sometimes replaced along the rim by green amphibole. The apatite occurs in almost all the samples and it displays a cloudy core full of CO_2-rich fluid inclusions (verified via micro-Raman spectroscopy). Rutile and ilmenite in the matrix are often coarse grained, with rutile rimmed by ilmenite.

5 | RESULTS

5.1 | Petrography of nanogranitoids and glassy inclusions

Two types of MI have been identified in garnet based on their microstructural distribution (Figure 4). The first type is dominant and occurs as a cluster in the inner part of the garnet (Figure 4a–d). The random distribution suggests that these MI are primary, thus they were trapped while the garnet was growing (Borghini et al., 2018). The second type of polycrystalline MI was recognized only in three RUB samples and it occurs in trails that cross-cut the crystal and the cluster of primary MI (Figure 4a–e). They post-date the garnet formation, thus they can be interpreted as secondary (Cesare, Acosta-Vigil, Bartoli, & Ferrero, 2015; Ferrero, Godard, Palmieri, Wunder, & Cesare, 2018). For the purpose of this paper we will focus exclusively on the primary inclusions.

Primary MI are either fully glassy or crystallized as nanogranitoids (Cesare et al., 2015). Glassy inclusions, 2–5 μm in diameter, were identified only in RUB samples and are isotropic under crossed polarizers. They occur in the same cluster with the nanogranitoids but represent just a modest fraction (<10%) of the inclusions occurring in the cluster, and they are generally smaller (Figures 4c and 5d). Their shape varies from isometric to prismatic and often they contain rutile. Nanogranitoids, 5–20 μm in diameter, were identified in both localities. They are mostly brown under plane-polarized light, and have a well-developed negative crystal shape, in some cases with minor cracks that do not reach the garnet borders (Figure 5a–c). The mineral assemblage is kumdykolite or albite, phlogopite/biotite, osumilite, and kokchetavite, with a variable amount of quartz, pyroxene, carbonate, and rare white mica (Figures 5 and 6; see also Borghini et al., 2018). Kokchetavite and carbonate are generally more abundant in RUB samples, whereas osumilite, pyroxene, and white mica occur more often in KLA. Kumdykolite, the orthorhombic polymorph of $NaAlSi_3O_8$, and kokchetavite, the hexagonal polymorph of $KAlSi_3O_8$, were reported for the first time together in nanogranitoids by Ferrero, Ziemann, Angel, O'Brien, and Wunder (2016). $NaAlSi_3O_8$ is present mainly as kumdykolite rather than
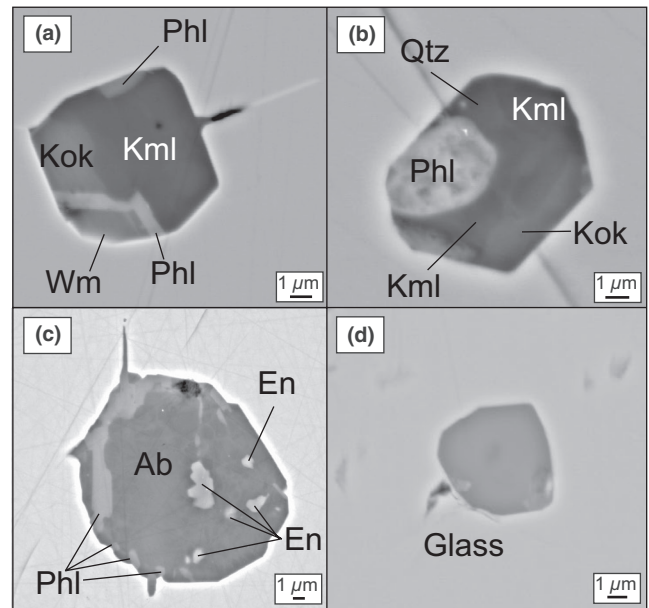

FIGURE 5 Backscattered electron images of nanogranitoids and a glass inclusion with a well-developed negative crystal shape. (a) Nanogranitoid containing kumdykolite (Kml), kokchetavite (Kok), phlogopite (Phl), and white mica (Wm) with a crack of limited extension that does not reach the rim of the host crystal. (b) Nanogranitoid that contains also quartz (Qtz), the line crossing the inclusion is not a crack but due to polishing, (c) nanogranitoids with phlogopite, enstatite (En), and albite (Ab), and a crack of limited extension that, as for (a), does not reach the rim of the crystal. (d) Glassy inclusions with a dark spot in the centre due to the microprobe beam damage

albite (triclinic), with the latter being present mostly in inclusions showing noticeable cracks. Phlogopite forms euhedral to subhedral lamellae and often nucleates on the inclusion walls (Figures 5a–c and 6b). Osumilite crystals often extend from wall to wall and do not develop an euhedral shape. Kokchetavite has commonly a prismatic elongated shape but in some MI it is anhedral and crystals often grow associated with kumdykolite. Plagioclase may occur instead of kumdykolite in subhedral tabular crystals. Quartz is always anhedral and interstitial, whereas pyroxene (mostly enstatite) is generally subhedral with a prismatic, locally stubby shape. White mica, commonly associated with phlogopite, is mainly subhedral. Overall, nanogranitoids show the following crystallization sequence based on the microstructural features of the phases in the inclusions: biotite, pyroxene, white mica, kumdykolite/albite and kokchetavite, osumilite, and quartz.

5.2 | Bulk rock geochemistry

The bulk rock composition has been analysed in three samples from each locality (see average values in Table 1 and
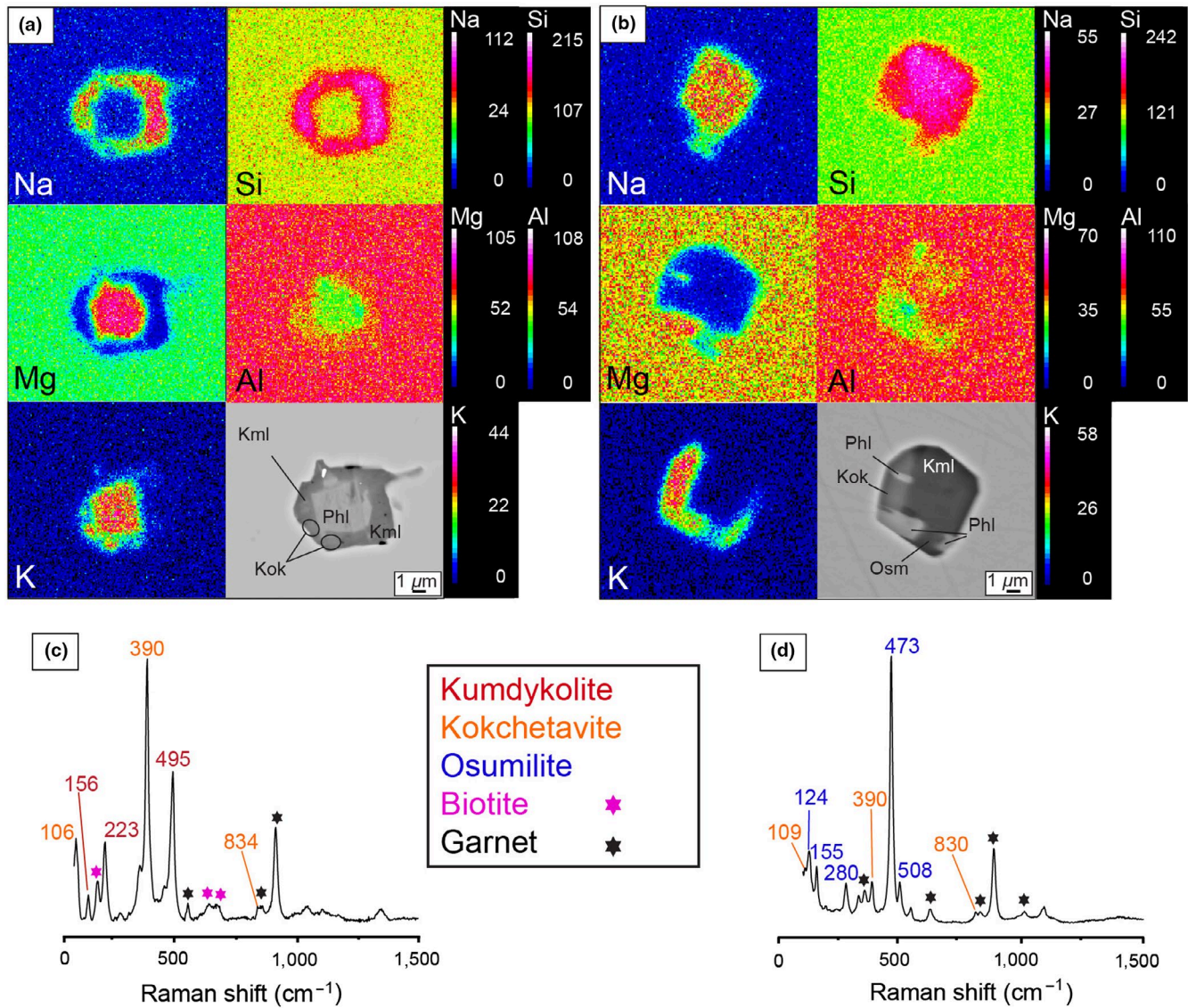
FIGURE 6 (a, b) EDS elemental maps of nanogranitoids with (a) kumdykolite, phlogopite, and kokchetavite, and (b) kumdykolite, phlogopite, kokchetavite, and osumilite (Osm). (c, d) Raman spectra of (c) kumdykolite and kokchetavite, and (d) osumilte and kokchetavite

complete data set in Table S1). Most, although not all, elements show similar abundances in both localities, for example, Al_2O_3, CaO, MgO, and MnO. SiO_2 is higher in KLA samples (46.07 wt% vs. 43.93 wt%), whereas FeO and TiO_2 contents are higher in those from RUB (FeO: 14.16 wt% vs. 11.62 wt%; TiO_2: 1.57 wt% vs. 0.77 wt%) and Na_2O is generally high in both with respect to a typical pyroxenite (RUB 1.59 wt% vs. KLA 2.22 wt%). The magnesium number (Mg#=[molar $Mg/(Mg+Fe^{2+}_{tot}) \times 100$]) is slightly lower in RUB (58) than in KLA (61) samples. The geochemistry of RUB and KLA samples can be compared with the extensively studied pyroxenites and eclogites in the peridotite bodies of the Gföhl Unit in the Moldanubian Zone as well as with other standard compositions such as N-MORB (data from Workman & Hart, 2005) (Table 1 and Figure 7). Although pyroxenites and eclogite are present across the whole Bohemian Massif, those from Mohelno, Horní Bory, and Nové Dvory

were selected for the comparison because these three localities gave their names to the three different types of peridotite of the Moldanubian Zone, as classified by Medaris, Wang, Jelínek, Mihaljevič, & Jakeš (2005) based on their chemical features. The SiO_2 content in the RUB and KLA samples is in the range defined by the whole data set (43–52 wt%). The Al_2O_3 and MgO contents are similar to those of kyanite eclogite and N-MORB, whereas they are higher and remarkably lower, respectively, than for the whole data set of Moldanubian pyroxenites. The CaO content of the investigated pyroxenites is instead lower than the kyanite eclogite, and closer to that of the Horní Bory pyroxenite, which has the highest CaO among the Moldanubian pyroxenites and average N-MORB. The RUB and KLA samples show the lowest Mg# of the whole investigated data set, whereas other oxides are higher, for example, FeO in both localities, TiO_2 in RUB and Na_2O in KLA.

TABLE 1 Whole-rock major and trace element composition of Rubinberg and Klatschmühle eclogites compared with the Moldanubian pyroxenite (Mohelno, Horní Bory, and Nové Dvory) and kyanite eclogite and N- and E-MORB (LOI = loss on ignition). List of selected samples and related references: average of RUB, RUB 6, and RUB 11 for Rubinberg (this study), average of KLA, KLA 1-2.1, and KLA 2.2 for Klatschmühle (this study), average of CZ3E and 11MO5C for Mohelno (Svojtka et al., 2016), HB63 for Horní Bory (Svojtka et al., 2016), average of LAND 1 and CS-ND-3B for Nové Dvory 1 (ND1; Svojtka et al., 2016), LAND 3 for Nové Dvory 2 (ND2; Svojtka et al., 2016), average of ND141, ND142, and ND143 for Nové Dvory 3 (ND3; Obata et al., 2006), N-MORB (Workman & Hart, 2005 for major and Sun & McDonough, 1989 for the trace elements), E-MORB (Sun & McDonough, 1989), low- and high-SiO_2 adakite (Martin et al., 2005), average of preserved glassy inclusions in 3.1 and 3.1 C for Rubinberg melt inclusions and average of re-homogenized nanogranitoids in Exp 1 and Exp 4 for the melt inclusions of Klatschmühle (all reported in the Data Repository of Borghini et al., 2018) and melt in mantle xenolith in arc lavas (Schiano et al., 1995)

Locality	Rubinberg Granulitgebirge (BM)	Klatschmühle Granulitgebirge (BM)	Mohelno Gföhl Unit (BM)	Horní Bory Gföhl Unit (BM)	Nové Dvory Gföhl Unit (BM)			N-MORB	E-MORB	Low-SiO_2 adakite	High-SiO_2 adakite	Rubinberg Granulitgebirge (BM)	Klatschmühle Granulitgebirge (BM)	Batan island, Luzon Arc (Philippines)
Sample type	Grt-clinopyroxenite	Grt-clinopyroxenite	Spl-websterite	Ol Grt-clinopyroxenite	ND1: Grt-clinopyroxenite	ND2: Grt-websterite	ND3: Kyanite eclogite	N-MORB	E-MORB	Low-SiO_2 adakite	High-SiO_2 adakite	Granitic melt	Granitic melt	Melt in mantle xenoliths in arc lavas
	Bulk	Bulk	Bulk	Bulk	Bulk	Bulk	Bulk	Bulk	Bulk	Bulk	Bulk	MI	MI	MI
No. analyses	3	3	2	1	2	1	3	267	77	267		7	6	12
wt%														
SiO_2	43.93	46.07	44.45	47.65	43.61	52.15	48.60	49.51	—	56.25	64.8	70.95	64.85	59.22
TiO_2	1.57	0.77	0.11	0.45	0.14	0.22	0.29	0.90	—	1.49	0.56	0.03	0.14	0.19
Al_2O_3	15.57	16.40	5.36	4.89	11.36	5.96	17.58	16.75	—	15.69	16.64	16.84	18.28	17.72
Fe_2O_3	0.00	0.00	3.53	1.73	2.26	1.37	0.00	—	—	—	—	0.00	0.00	—
FeO	14.16	11.62	3.65	5.53	3.96	4.04	5.09	8.05	—	6.47	4.75	0.56	1.60	2.62
MnO	0.24	0.18	0.12	0.14	0.15	0.13	0.10	0.14	—	0.09	0.08	0.03	0.07	0.09
MgO	11.23	10.11	30.89	23.13	23.38	22.73	10.81	9.74	—	5.15	2.18	0.22	0.99	0.79
CaO	12.05	11.89	3.89	12.99	7.07	10.34	14.94	12.50	—	7.69	4.63	0.43	1.55	4.05
Na_2O	1.59	2.22	0.25	0.44	0.37	0.51	1.80	2.18	—	4.11	4.19	5.43	5.52	4.16
K_2O	0.07	0.42	0.02	0.01	0.02	0.04	0.04	0.07	—	2.37	1.97	5.06	5.40	2.94
P_2O_5	0.12	0.16	0.02	0.02	0.04	0.03	0.04	0.10	—	0.66	0.2	0.03	0.27	0.40
LOI	0.12	0.29	7.33	2.64	7.32	2.07	—	—	—	—	—	—	—	—
Total	100.64	100.13	99.59	99.62	99.65	99.59	99.28	99.93	—	99.97	100.00	99.57	98.67	92.18
ASI										0.67	0.95	1.12	1.04	1.02
CaO/Al_2O_3	0.77	0.73	0.73	2.66	0.62	1.73	0.85	0.75	—	0.49	0.28	0.03	0.08	0.23
Mg#	58	61	89	85	88	89	79	71	—	58	45	32	50	34
ppm														

(Continues)

TABLE 1 Continued

Locality	Rubinberg Granulitgebirge (BM)	Klatschmühle Granulitgebirge (BM)	Mohelno Gföhl Unit (BM)	Horní Bory Gföhl Unit (BM)	Nové Dvory Gföhl Unit (BM)					Low-SiO₂ adakite	High-SiO₂ adakite	Rubinberg Granulitgebirge (BM)	Klatschmühle Granulitgebirge (BM)	Batan island, Luzon Arc (Philippines)
					ND1: Grt-clinopyroxenite	ND2: Grt-websterite	ND3: Kyanite eclogite	N-MORB	E-MORB			Granitic melt	Granitic melt	Melt in mantle xenoliths in arc lavas
Sample type	Grt-clinopyroxenite	Grt-clinopyroxenite	Spl-websterite	Ol Grt-clinopyroxenite										
	Bulk	Bulk	Bulk	Bulk	Bulk	Bulk	Bulk	Bulk	Bulk	Bulk	Bulk	MI	MI	MI
No. analyses	3	3	2	1	2	1	3			77	267	7	6	12
Cr	367	500	—	—			780			157	41	—	—	37
Ni	91	74	1,361	878	660	755	113			157	20	—	—	—
Rb	8.13	22	1.87	0.88	0.79	1.62	3.98	0.56	5.04	19	52	176[a]	265[a]	—
Cs	22	21	0.37	0.09	0.05	0.34	0.28	0.01	0.06	—	—	45	63	—
Ba	139	142	9.14	2.22	14	162	28	6.30	57	1,087	721	678	403	—
Th	1.50	0.60	0.07	0.14	0.12	0.68	b.d.l.	0.12	0.60	—	—	105	39	—
U	1.03	0.20	0.03	0.08	0.07	0.10	b.d.l.	0.05	0.18	—	—	23	13	—
Nb	11	6.53	0.22	0.34	0.17	1.24	0.59	2.33	8.30	11	6.00	2.75	4.08	7.92
Ta	0.83	0.70	—	—	—	—	—	0.13	0.47	—	—	1.01	0.85	—
La	9.20	9.67	0.35	0.80	0.74	5.08	0.34	2.50	6.30	41	19	23	11	51
Ce	21	22	0.80	2.36	2.33	14	1.17	7.50	15	90	38	39	24	81
Pb	4.07	1.60	1.53	2.13	1.08	3.73	—	0.30	0.60	—	—	59	36	—
Pr	2.86	3.00	0.11	0.43	0.39	1.95	0.25	1.32	2.05	—	—	3.48	3.23	—
P	1,167	1,633	150	200	350	300	367	510	620	—	—	670	460	—
Sr	98	153	10	65	48	138	109	90	155	2,051	565	126	128	552
Nd	13	14	0.61	2.55	2.28	8.38	1.29	7.30	9.00	47	18	10	11	19
Zr	69	65	2.84	11	12	18	9.30	74	73	188	108	68	169	186
Hf	2.10	2.13	0.14	0.50	0.40	0.62	0.28	2.05	2.03	—	—	3.71	5.20	—
Sm	3.79	3.70	0.23	0.96	0.95	1.66	0.61	2.63	2.60	7.80	3.40	6.51	4.07	2.51
Eu	1.11	1.09	0.09	0.36	0.27	0.40	0.36	1.02	0.91	2.00	0.90	3.15	2.10	—
Gd	4.88	4.23	0.41	1.42	1.64	1.52	0.74	3.68	2.97	4.80	2.80	—	—	—
Tb	0.90	0.66	0.08	0.25	0.38	0.22	0.17	0.67	0.53	—	—	—	—	—
Dy	5.91	3.71	0.60	1.58	3.00	1.25	1.13	4.55	3.55	2.80	1.90	—	—	1.06
Ti	15,700	7,667	1,050	4,500	1,400	2,200	287	7,600	6,000	—	—	3,105	1,454	1,140
Y	34	19	5.46	8.87	21	8.52	6.59	28	22	13	10	—	—	5.92
Ho	1.33	0.72	0.14	0.31	0.75	0.22	0.27	1.01	0.79	—	—	—	—	—

(Continues)

TABLE 1 Continued

Locality	Rubinberg Granulitgebirge (BM)	Klatschmühle Granulitgebirge (BM)	Mohelno Gföhl Unit (BM)	Horní Bory Gföhl Unit (BM)	Nové Dvory Gföhl Unit (BM)			N-MORB	E-MORB	Low-SiO₂ adakite	High-SiO₂ adakite	Rubinberg Granulitgebirge (BM)	Klatschmühle Granulitgebirge (BM)	Batan island, Luzon Arc (Philippines)
Sample type	Grt-clinopyroxenite	Grt-clinopyroxenite	Spl-websterite	Ol Grt-clinopyroxenite	ND1: Grt-clinopyroxenite	ND2: Grt-websterite	ND3: Kyanite eclogite	N-MORB	E-MORB	Low-SiO₂ adakite	High-SiO₂ adakite	Granitic melt	Granitic melt	Melt in mantle xenoliths in arc lavas
	Bulk	Bulk	Bulk	Bulk	Bulk	Bulk	Bulk	Bulk	Bulk	Bulk	Bulk	MI	MI	MI
No. analyses	3	3	2	1	2	1	3			77	267	7	6	12
Er	4.07	1.91	0.43	0.87	2.57	0.67	0.67	2.97	2.31	1.12	0.96	—	—	—
Tm	0.58	0.25	0.06	0.12	0.42	0.09	0.10	0.46	0.36			—	—	—
Yb	3.78	1.52	0.45	0.73	2.91	0.58	0.70	3.05	2.37	0.93	0.88	—	—	0.69
Lu	0.57	0.22	0.07	0.10	0.45	0.09	0.10	0.46	0.35	0.08	0.17	—	—	—
Li	n.d.	n.d.	5.67	3.24	11.22	4.67		4.30	3.50			50	52	—
B	n.d.	n.d.										70	58	—

Abbreviations: b.d.l., below detection limit; LOI, loss on ignition; n.d., not determined.

ᵃThe trace element averages of the melt are the maximum averages.

The trace element patterns of RUB and KLA samples are similar (Table 1 and Figure 8). They both contain high amounts of Large Ion Lithophile Elements (LILE; Rb, Cs, and Ba in addition to K) with a very strong Cs-positive anomaly, a positive anomaly for U, Ti, and to a lesser extent Ta, and a slightly negative anomaly for Pb. RUB samples are richer in Cs, U, Nb, Ta, and Ti than the KLA ones and show a negative Sr anomaly. The rare earth element (REE) patterns for samples from both localities show no to weak fractionation with KLA samples slightly more fractionated with respect to RUB. For RUB samples, the pattern is almost flat with a slightly higher amount of light rare earth elements (LREEs) with respect to the heavy rare earth elements (HREEs) with average $La_N/Yb_N = 1.87$, whereas KLA samples have the same LREE content as RUB ones but show a slight depletion in HREEs, resulting in average $La_N/Yb_N = 4.36$. Samples from both localities have a slightly negative Eu anomaly, and Eu_N/Eu^* ratios $[Eu_N/Eu^*=Eu_N/\sqrt{(Sm_N*Gd_N)}]$ are 0.79 for RUB and 0.84 for KLA. The trace element patterns have been compared with the same data set used for the major elements plus E-MORB (Figure 8; data from Sun & McDonough, 1989). The LILE enrichment and the positive U and Ti anomaly are peculiar features of RUB and KLA samples, whereas the negative Pb anomaly is similar to both MORB compositions but completely absent in the data set of selected Moldanubian rocks, which rather shows instead a clear positive anomaly (Figure 8a). Among the REEs, the LREE patterns in RUB and KLA samples are similar to E-MORB but their concentrations are higher than all the other rocks, whereas the HREEs are more abundant in RUB rocks and slightly more depleted in KLA samples when compared with the rest of the Moldanubian pyroxenites and both MORB compositions (Figure 8b).

5.3 | Mineral chemistry

The main minerals in the rock representing the high-PT stage of the evolution are garnet and clinopyroxene. The major and trace elements for these phases are plotted in Figures 7 and 9, where they are compared with whole rock and mineral analyses from comparable rocks from other parts of the Bohemian Massif (the whole data set is reported in Tables 2 and 3 and in Tables S2–S4).

5.3.1 | Garnet

In the RUB sample, garnet is in average pyrope (Prp) 39, almandine (Alm) 35, spessartine (Sps) 1, and grossular (Grs) 25 with Mg# = 55. By contrast, in Klatschmühle, the samples can be divided into two groups based on the different garnet compositions: $Prp_{66}Alm_{24}Sps_0Grs_{10}$ (KLA 1) with an Mg# =74 and $Prp_{37}Alm_{35}Sps_1Grs_{27}$ (KLA 2) with

an Mg# = 52. In all cases, a thin rim with lower Grs and higher Prp and Alm is discernible (see Fig. S1). Garnet from RUB and KLA 2 samples contain less Prp and a lower Mg# with respect to garnet in the Moldanubian garnet pyroxenites ($Prp_{57-71}Alm_{15-21}Sps_{0-1}Grs_{12-22}$; Mg# = 73–82; Svojtka et al., 2016), whereas garnet from specimen KLA 1 is very similar but with a lower Grs and higher Alm content. MI occur in the core of garnet in the RUB, KLA1, and KLA2 samples. Despite showing some compositional differences, both high-Prp and low-Prp garnet contain MI of essentially the same composition.

Normalized REE patterns of garnet (Figure 9a) are similar for the LREEs: both are depleted with a Ce_N/Yb_N ratio between 0.01 and 0.18. In RUB samples, the relative content of medium rare earth elements (MREEs, from Gd

to Dy) with respect to the LREEs is correlated with the Eu anomaly (expressed as the ratio Eu_N/Eu^*). When the anomaly is positive (Eu_N/Eu^* = 1.26), MREEs are more abundant than HREEs, whereas when the anomaly is negative (Eu_N/Eu^* = 0.87) the amount of MREEs is similar to HREEs and the pattern is flatter. In specimen KLA 1, the Eu anomaly is slightly negative (Eu_N/Eu^* = 0.93) or absent and the content of MREEs is higher than HREEs. Furthermore, despite the compositional difference in major elements and in the HREEs, the garnet in the two localities have similar trace element patterns (Figure 9c). They are generally depleted in LILE, Nb, and Hf, and display negative Sr and Ti anomalies and positive Th, U, and Zr anomalies. Comparison with the trace elements of the Moldanubian data set shows that RUB and KLA garnet

FIGURE 7 Variation in the major oxides relative to the wt% MgO of whole rock (see Table 1, Table S1 and supporting information; Borghini et al., 2018), constituent minerals (Grt and Cpx) and melt inclusions of Rubinberg (RUB) and Klatschmühle (KLA) eclogite. They are compared with the pyroxenites (Mohelno, Horní Bory, and Nové Dvory; from Svojtka et al., 2016) and kyanite eclogite (Obata et al., 2006) of the Gföhl Unit in the Moldanubian Zone (original data reported in Table 1), N-MORB (Workman & Hart, 2005; Table 1), and primitive mantle (PM; McDonough & Sun, 1995)
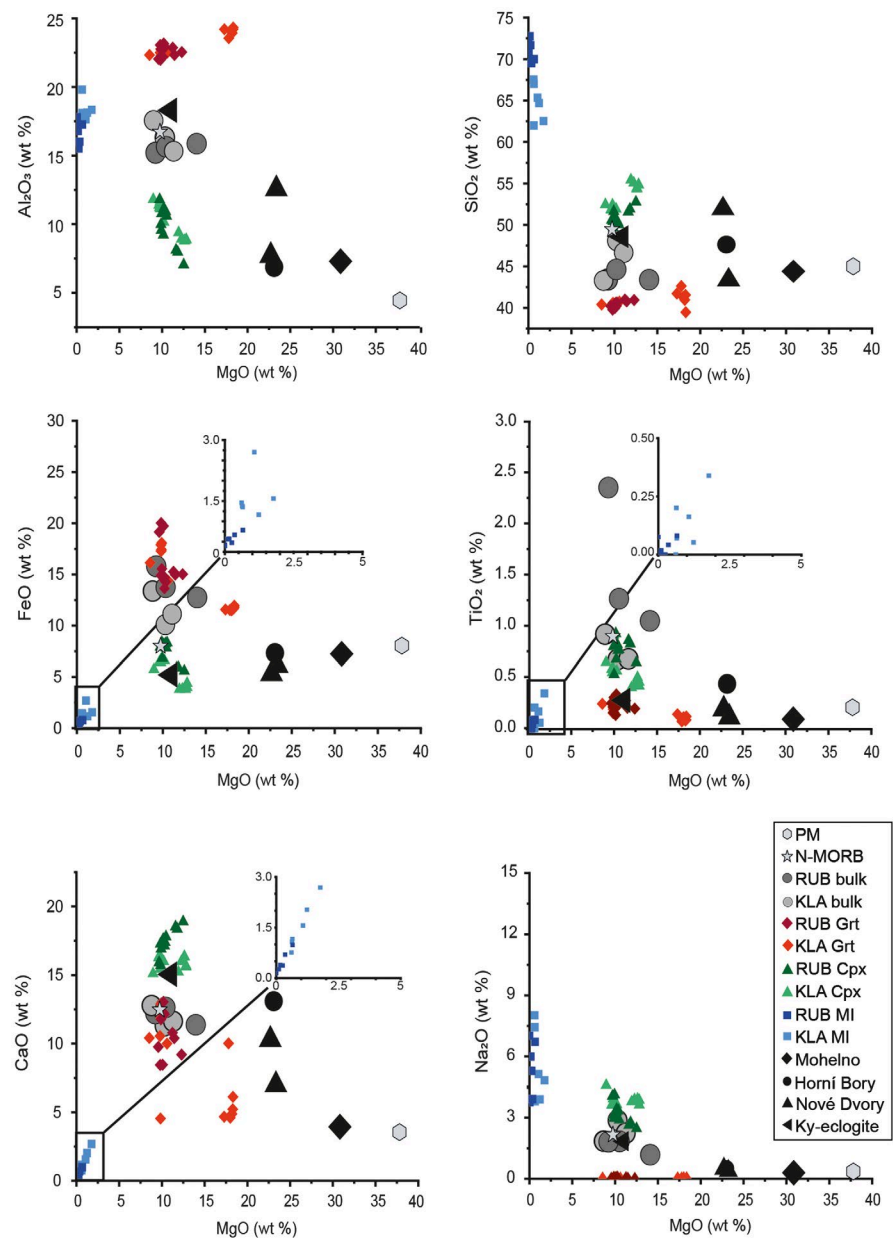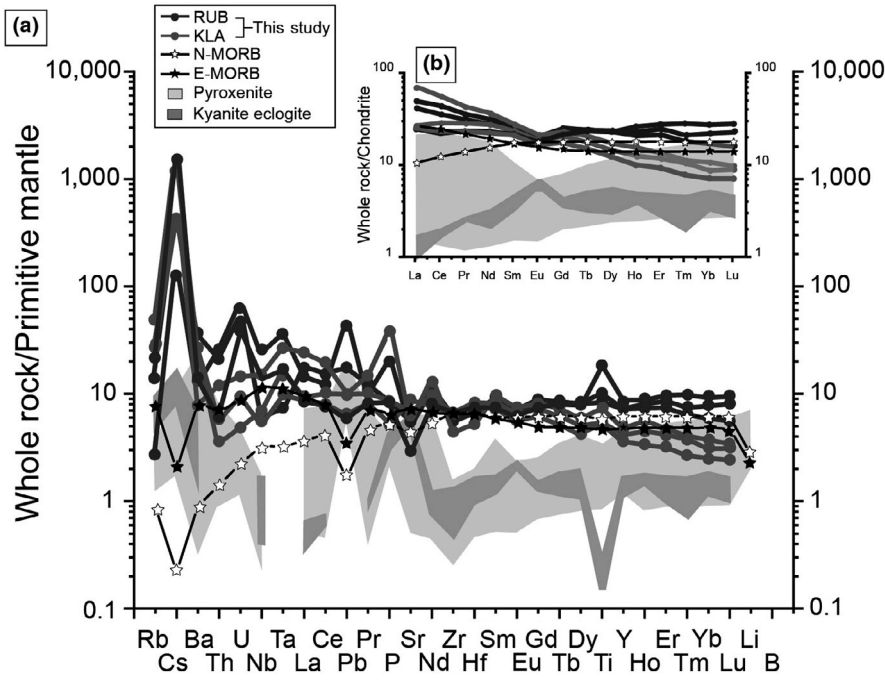
FIGURE 8 Whole-rock trace element patterns (a) and rare earth element (REE) patterns (b) of RUB and KLA (Table 1, Table S1 and Data Repository of Borghini et al., 2018) compared with the whole data set of the Moldanubian pyroxenite and eclogite (references for the data used in the plot are reported in the caption to Figure 7) and the N- and E-MORB (both from Sun & McDonough, 1989). All the trace element data have been normalized to primitive mantle (Sun & McDonough, 1989, except for B, which is taken from McDonough & Sun, 1995), whereas the REEs have been normalized to chondrite (Sun & McDonough, 1989)
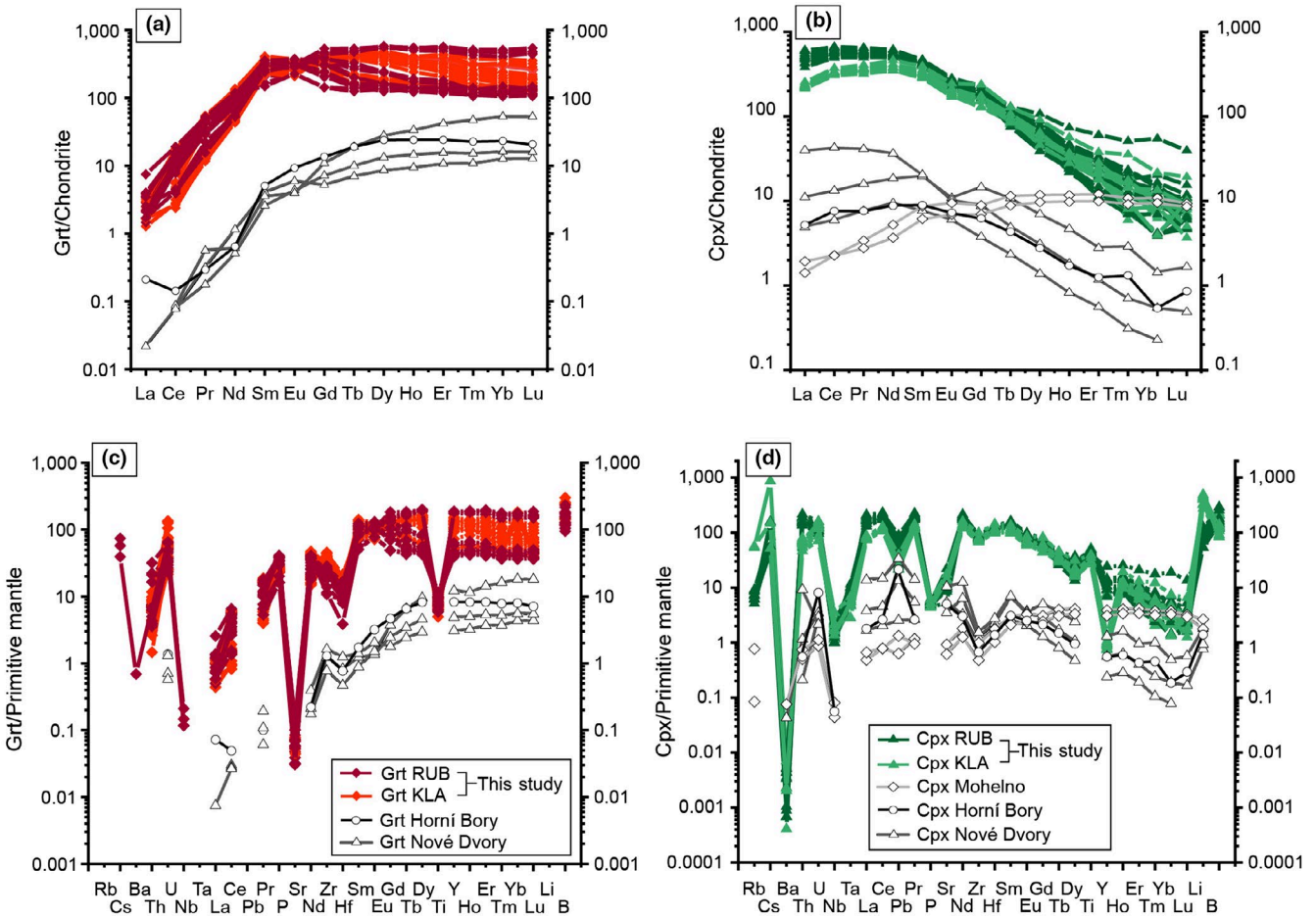

FIGURE 9 REE patterns of RUB and KLA garnet (a) and clinopyroxene (b) (see Tables S2 and S3, respectively) compared with the pyroxenite of the Gföhl Unit in the Moldanubian Zone (same data Figure 7) and trace element patterns of RUB and KLA garnet (c) and clinopyroxene (d) compared with the same pyroxenite. For normalized values see the caption to Figure 8

TABLE 2 Representative garnet and clinopyroxene electron microprobe analyses of Rubinberg and Klatschmühle eclogites

Locality	Rubinberg		Klatschmühle			Rubinberg		Klatschmühle	
Phase	Garnet					Clinopyroxene			
Sample name	RUB		KLA 1	KLA 2		RUB		KLA 1	KLA 2
wt%									
SiO_2	40.26	40.99	41.31	40.24		50.41	52.00	54.45	51.89
TiO_2	0.30	0.27	0.11	0.18		0.76	0.82	0.42	0.55
Al_2O_3	22.74	22.86	24.10	22.48		10.97	8.01	8.82	11.64
Fe_2O_3	—	—	—	—		—	—	—	—
FeO	15.55	15.26	11.49	17.28		7.80	5.89	3.80	6.41
MnO	0.27	0.33	0.19	0.34		0.07	0.06	0.02	0.05
MgO	9.88	11.23	18.00	9.80		10.38	11.80	12.62	9.75
CaO	11.77	10.79	4.88	10.41		17.41	18.37	16.32	16.44
Na_2O	0.08	0.04	0.05	0.03		3.36	2.77	3.91	4.03
K_2O	0.00	0.00	0.00	0.00		0.01	0.00	0.06	0.01
P_2O_5	0.10	0.06	0.05	0.06		0.01	0.01	0.01	0.00
Total	100.95	101.84	100.18	100.83		101.17	99.74	100.43	100.77
Mg#	53	57	74	50		70	78	86	73
Si	2.99	3.00	2.96	3.00	Si	1.82	1.90	1.94	1.86
					Al IV	0.18	0.10	0.06	0.14
Ti	0.02	0.01	0.01	0.01	Fe^{3+}	0.00	0.00	0.00	0.00
Al	1.99	1.97	2.04	1.98	Cations T	2.00	2.00	2.00	2.00
	2.01	1.98	2.04	1.99	Al VI	0.28	0.24	0.31	0.36
					Fe^{3+}	0.10	0.01	0.00	0.03
Fe	0.97	0.93	0.69	1.08	Ti	0.02	0.02	0.01	0.01
Mn	0.02	0.02	0.01	0.02	Cr	0.00	0.00	0.00	0.00
Mg	1.09	1.22	1.93	1.09	Mg	0.56	0.64	0.67	0.52
Ca	0.94	0.85	0.38	0.83	Fe^{2+}	0.14	0.17	0.11	0.16
	3.01	3.02	3.00	3.02	Mn	0.00	0.00	0.00	0.00
					Cations M1	1.09	1.09	1.10	1.09
					Ca	0.67	0.72	0.62	0.63
					Na	0.23	0.20	0.27	0.28
					Cations M2	0.91	0.91	0.89	0.91
mol.%					mol.%				
Alm	32	31	23	36					
Prp	36	40	64	36	Jd	19	19	28	27
Sps	1	1	0	1	Quad	74	80	72	70
Grs	31	28	13	28	Ae	7	1	0	2

Note: For the garnet: Alm = almandine; Prp = pyrope; Sps = spessartine and Grs = grossular. For the clinopyroxene: Jd = jadeite; Quad = quadrilateral (Ca–Mg–Fe^{2+} pyroxenes) and Ae = aegirine.

have higher general enrichment in trace elements, a content of LREEs almost two orders of magnitude higher, and in addition the HREEs show a much flatter normalized pattern. Mohelno-type pyroxenites are not reported because they are garnet-free (Figure 9a–c).

5.3.2 | Clinopyroxene

As for the garnet, clinopyroxene shows variations in composition not only between the two localities but also within a single sample (Figure 7). In RUB samples

TABLE 3 Representative garnet and clinopyroxene LA-ICP-MS analyses of Rubinberg and Klatschmühle eclogite

Locality	Rubinberg		Klatschmühle		Rubinberg		Klatschmühle	
	Garnet				Clinopyroxene			
Name	1	2	3	4	1	2	3	4
ppm								
Rb	b.d.l.	b.d.l.	b.d.l.	b.d.l.	3.90	3.29	b.d.l.	b.d.l.
Cs	b.d.l.	b.d.l.	b.d.l.	b.d.l.	1.42	1.81	b.d.l.	1.66
Ba	b.d.l.	b.d.l.	b.d.l.	b.d.l.	6.19	30	b.d.l.	16
Th	0.62	0.54	0.77	0.51	14	16	4.50	6.75
U	1.22	1.37	1.28	1.26	2.45	2.69	1.51	2.68
Nb	b.d.l.	b.d.l.	0.11	b.d.l.	0.95	0.73	1.35	1.19
Ta	b.d.l.	b.d.l.	b.d.l.	b.d.l.	0.42	0.37	b.d.l.	0.19
La	0.81	0.82	b.d.l.	b.d.l.	91	116	54	60
Ce	10.2	9.54	2.58	3.40	303	351	201	228
Pb	b.d.l.	b.d.l.	b.d.l.	b.d.l.	7.50	8.39	4.11	7.26
Pr	4.53	4.42	1.45	1.22	47	53	36	39
P	3,326	3,184	2,219	2,169	419	487	441	575
Sr	1.57	1.25	b.d.l.	b.d.l.	111	183	292	366
Nd	55	49	22	24	232	258	179	216
Zr	227	231	502	493	850	901	776	1,114
Hf	3.88	3.75	5.78	5.62	34	37	33	44
Sm	55	51	39	34	63	66	47	60
Eu	18	19	15	16	14	15	11	14
Gd	42	43	78	74	44	41	33	49
Tb	5.35	5.68	15	15	4.88	4.28	3.00	4.81
Dy	35	31	111	111	27	18	13	23
Ti	12,934	12,846	6,466	8,376	49,549	58,851	35,106	51,013
Y	179	182	621	596	110	65	4.43	6.19
Ho	6.84	7.54	23	22	4.16	2.57	1.73	3.20
Er	21	21	73	60	10.01	5.20	3.44	6.28
Tm	3.02	2.74	9.59	7.92	1.31	0.54	0.57	0.91
Yb	21	22	63	50	9.34	2.81	1.12	3.68
Lu	2.93	2.83	8.99	6.60	1.00	0.30	0.12	0.49
Li	b.d.l.	b.d.l.	b.d.l.	b.d.l.	87	149	511	534
B	65	53	42	b.d.l.	43	54	27	33

Abbreviation: b.d.l., below detection limit.

the clinopyroxene is generally a sodic diopside with Mg# = 70–74 and an average jadeite (Jd) content of 19 mol.%, whereas in KLA samples it is an omphacite, Mg and Na richer, with Mg# = 73–85 and Jd = 28 mol.%. Within a single sample, Al_2O_3 and FeO in clinopyroxene show a negative correlation with MgO, whereas SiO_2 and CaO a positive one. TiO_2 and Na_2O contents are rather high for a pyroxenite *s.s.* (Svojtka et al., 2016; see also Discussion) and they show a negative correlation with MgO. RUB and KLA clinopyroxenes have lower Mg# and higher Jd content compared with the Moldanubian

data set (Mg# = 89–94; Jd = 3–18 mol.%; Svojtka et al., 2016).

The normalized clinopyroxene REE patterns are convex upward with HREE depletion in both samples (Figure 9b), but with LREE enrichment slightly greater in RUB than in KLA specimens. In both cases the Eu anomaly is slightly negative with a Eu_N/Eu^* of 0.89 and 0.86 for RUB and KLA samples, respectively. Trace element patterns are similar in the two localities (Figure 9d), and show enrichment in Cs, Rb, U, Th, and Li. By contrast, Nb, Ta, Pb, P, and Y show a weak negative anomaly, whereas the Ba anomaly is strong.
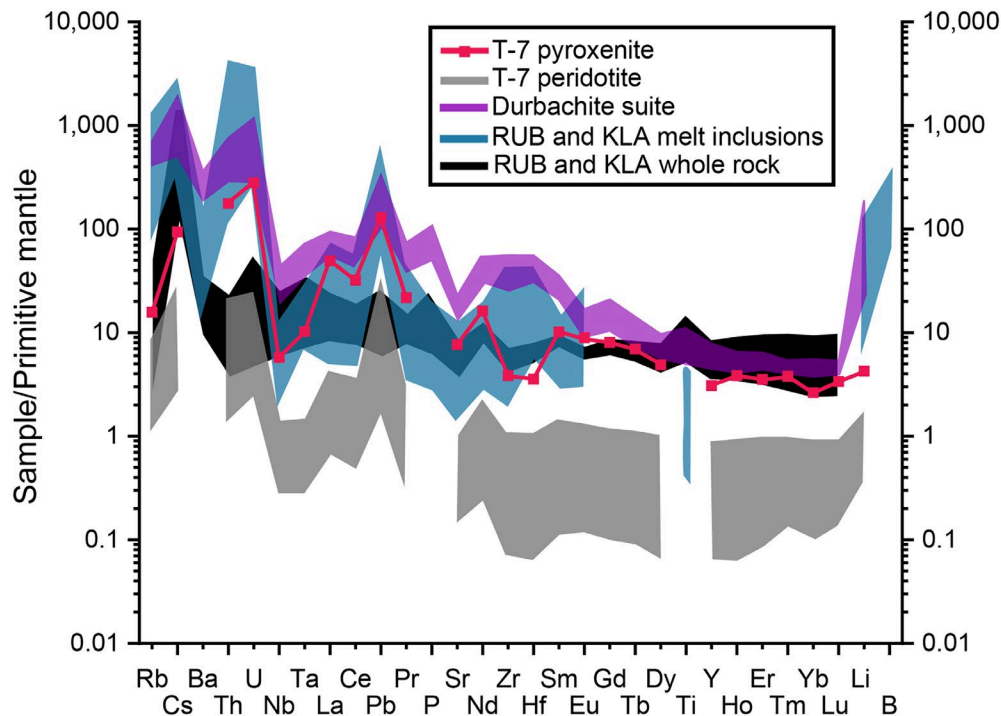
FIGURE 10 Trace element patterns of RUB and KLA melt inclusions compared with the whole-rock trace element patterns of RUB and KLA, the durbachite suite (Janoušek & Holub, 2007), and the peridotite and pyroxenite of the T-7 borehole (Medaris et al., 2015). For normalized values see the caption to Figure 8
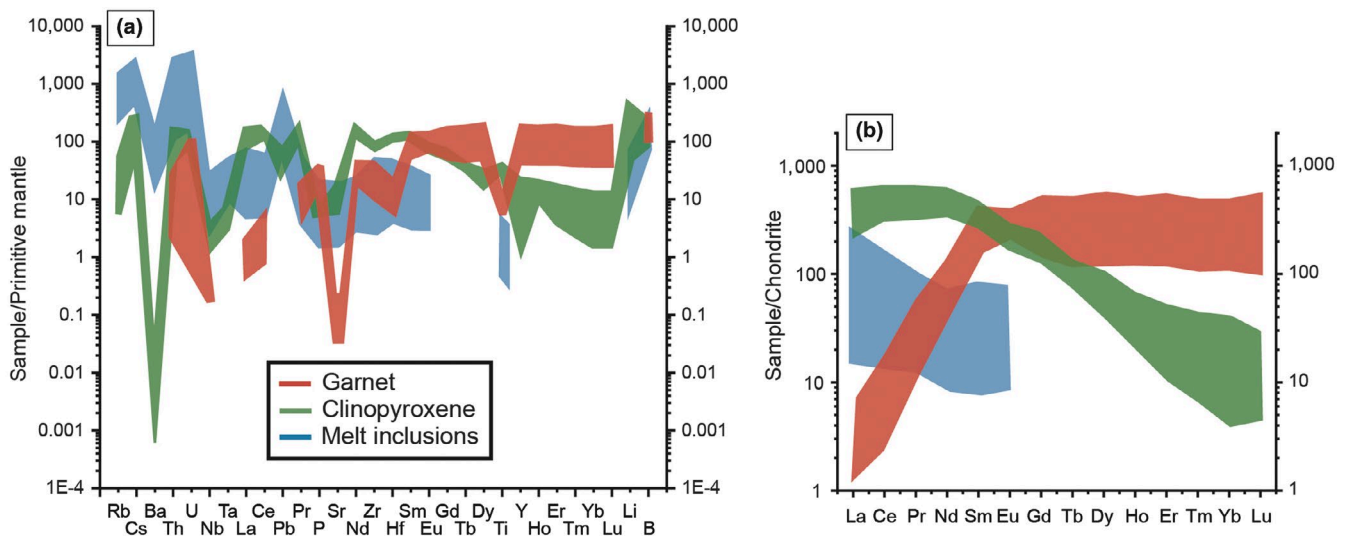

FIGURE 11 Trace element (a) and REE (b) composition patterns of garnet, clinopyroxene, and melt inclusions of RUB and KLA eclogites represented together. All the trace element data have been normalized to primitive mantle (Sun & McDonough, 1989 except for B from McDonough & Sun, 1995), whereas the REEs have been normalized to chondrite (Sun & McDonough, 1989)

RUB and KLA clinopyroxenes have higher LILE, Th, Li, and B with respect to those of the listed Moldanubian pyroxenites, whereas Pb and Y anomalies have the opposite trend. Their REE patterns are convex upward as for the Nové Dvory samples but with higher enrichment (almost two orders of magnitude). The pattern is instead the opposite of the Mohelno type, in which the clinopyroxene is richer in HREEs because of the absence of garnet (Figure 9d).

5.3.3 | Other phases

Plagioclase surrounding garnet and clinopyroxene is typically $Ab_{76}An_{22}Or_2$ and has a similar composition in all the different microstructural positions—interstitial, in leucocratic pockets or as lamellae or blebs along the clinopyroxene cleavage—as well as in the samples from both localities. The dominant brown amphibole, a hornblende with a composition between
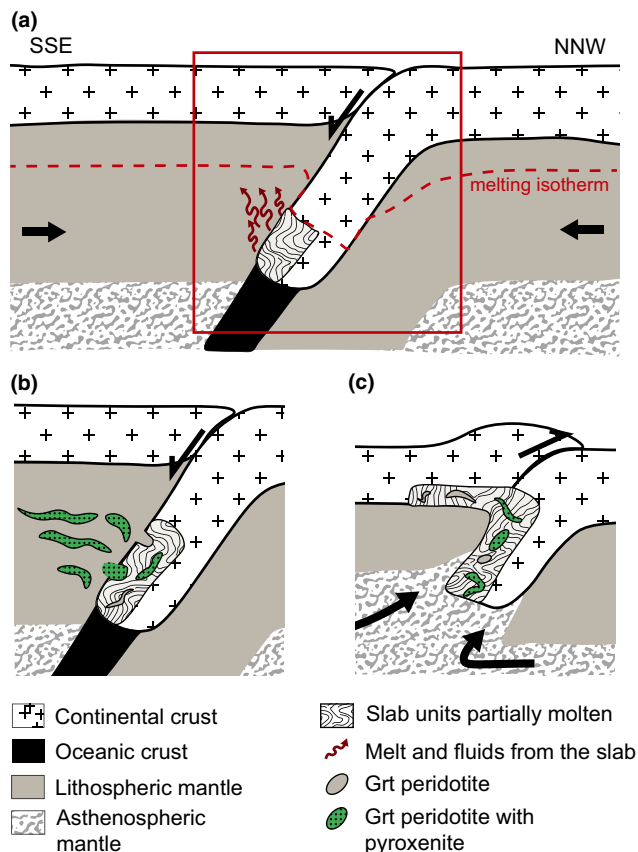
+ Continental crust
■ Oceanic crust
▨ Lithospheric mantle
▨ Asthenospheric mantle

▧ Slab units partially molten
↝ Melt and fluids from the slab
◯ Grt peridotite
● Grt peridotite with pyroxenite

FIGURE 12 Possible scenario for origin and evolution of the peridotite with pyroxenite in the geotectonic setting of the Granulitgebirge: (a) HP metamorphism, release of melt and fluids and metasomatism; (b) peridotite emplacement in the crust; and (c) subsequent exhumation of granulites and peridotite with and without pyroxenite. Based on Brueckner (1998); Janoušek and Holub (2007); Medaris et al. (2005); O'Brien (2000)

Mg-hastingsite and pargasite, contains 1.6 wt% TiO_2 and has Mg# of 70, whereas biotite is mainly a phlogopite with 3–3.5 wt% TiO_2 and an Mg# of 70 (RUB) or 85 (KLA) (see Table S4).

5.4 | MI chemistry

The major element composition of the MI in RUB and KLA 1 eclogite samples was already discussed in detail by Borghini et al. (2018; see data repository for analyses; Figure 7 and Table 1; see Table S5 for the trace element). As the samples RUB and KLA 2 are similar, this geochemical study concentrated on the contrasting samples RUB and KLA1. The melt is mainly granitic, hydrous, and alkali-rich in both localities. Contents of Al_2O_3, CaO, FeO, and TiO_2 correlate positively with MgO, whereas SiO_2 correlates slightly negatively (Figure 7). In terms of trace elements, the melt displays marked enrichment in LILE (Cs, Rb, to a lesser extent Ba), Th, U, Li, and B, and strong negative anomaly in Ti (partially below the primitive mantle values). The patterns reveal a strong positive anomaly in Pb and to a lesser extent Zr–Hf, and negative anomalies for Nb, Ta, and Sr (Figure 10). Despite the fact that the Th content is higher in RUB than in KLA 1 inclusions, the trends are very similar in both localities. The melt is also enriched in LREEs (Figure 11) with a La_N/Nd_N ratio higher in RUB (average 6.82) than in KLA 1 (average 2.47) samples.

6 | DISCUSSION

6.1 | The trapped melt and its origin

The melt trapped in the eclogitic bodies of Klatschmühle and Rubinberg in Granulitgebirge (Bohemian Massif) is granitic in composition, peraluminous, and slightly hydrous (<2 wt% H_2O, Table 1). The possibility that this is a supersilicic fluid can be ruled out because the water content in the latter is usually much higher (e.g. 25–50 wt%; Frezzotti, Ferrando, Dallai, & Compagnoni, 2007). The presence of kumdykolite and kokchetavite in the crack-free inclusions supports their chemical preservation (Ferrero et al., 2016; Ferrero, Godard,

TABLE 4 Schematic differences between garnet pyroxenite and eclogite

	Garnet pyroxenite	Eclogite	References
Whole rock			
Na_2O	≤0.7 wt%[a]	>0.8 wt%	Medaris et al. (1995), Medaris et al. (2006), Svojtka et al. (2016)
TiO_2	Lower	Higher	Medaris et al. (1995), Obata et al. (2006)
Cr	>0.15 wt%	<0.15 wt%	Medaris et al. (1995), Medaris et al. (2006), Obata et al. (2006)
Ni	>400 ppm	<400 ppm	Medaris et al. (1995), Medaris et al. (2006), Svojtka et al. (2016)
Mg#	>80	<80	Medaris et al. (1995)
Cpx	Augite–diopside or chrome diopside; no omphacite	Omphacite (Jd > 20–25 mol.%)	Carswell (1990), Medaris et al. (1995), Gonzaga et al. (2010), Obata et al. (2006)

[a]The Na content is the one reported by Svojtka et al. (2016) for most of the pyroxenites of the Moldanubian zone.

et al., 2018; Ferrero, O'Brien, et al., 2018) making it highly unlikely that the low H_2O content of the inclusions is the result of H_2O loss.

According to microstructural and geochemical evidences—that is, granoblastic texture (Figure 3c,d) and REE partitioning with high LREE abundance in clinopyroxene with the same enrichment factor of the HREEs in garnet (Figure 11b)—garnet and clinopyroxene formed at peak condition. The melt occurs as primary inclusions in garnet cores, thus, the melt was trapped at the metamorphic peak while garnet and clinopyroxene were growing at mantle depth, as already discussed in Borghini et al. (2018).

The melt trace element pattern suggests the involvement of white mica in the melting reaction (see also Acosta-Vigil et al., 2010), which likely occurred in the presence of an aqueous fluid responsible for the high amount of Th and U in the melt (Borghini et al., 2018). A Th-, U-rich phase consumed during melting of metasediments is often monazite (Hermann & Rubatto, 2009), but this should be visible in the melt in terms of extensive enrichment in LREEs with respect to Th and U, a feature absent in the investigated MI. Also, the strong positive Pb anomaly, the depletion in Ti, and the negative Nb anomaly (Figure 10) are all typical of a continental crust signature (Hartmann & Wedepohl, 1993). The source of the melt is thus most likely a phengite/muscovite-bearing rock belonging to the continental crust (either a meta-sediment or a meta-granitoid), subducted to mantle depth and melted in the presence of a Th-, U-rich fluid.

Crust–mantle interaction commonly generates adakites, that is, intermediate to felsic magmatic rocks considered the modern equivalent of the pristine continental crust (i.e. Trondjhemite, Tonalite and Granodiorite suite or TTG; Hastie et al., 2010; Martin, Smithies, Rapp, Moyen, & Champion, 2005). The melt hosted in the inclusions (Table 1) is very different from common adakitic melts: (a) it is significantly lower in FeO, MgO, CaO, and TiO_2 and richer in K_2O and Na_2O; (b) as for trace elements, the strong positive Sr anomaly and the Ba-positive anomaly relative to Rb, typical of adakites, are completely absent in RUB and KLA melt. Moreover, the generation of adakitic melts generally involves amphibole melting and proceeds via either (i) partial melting of the subducted oceanic slab with later melt enrichment in MgO, Cr, and Ni, and high Mg# because of interaction with the mantle wedge during ascent or (ii) partial melting of peridotite previously metasomatized by a felsic slab-derived melt (Martin et al., 2005). Both scenarios require amphibole melting, whereas the trapped melt is clearly enriched in elements characteristic of a melting reaction involving white mica (see discussion above).

A possible source for the melt trapped in the studied eclogites could be the Granulitgebirge granulites surrounding the peridotite, as they were already juxtaposed before the granulite

metamorphic peak (Schmädicke et al., 2010). This possibility was already ruled out by Borghini et al. (2018) because the melt generated by felsic granulite melting shows a different geochemical signature (Ferrero, O'Brien, et al., 2018). Moreover, the melt-bearing KLA eclogites formed at 380 Ma (von Quadt, 1993), whereas melting in the granulites was likely coeval to the HP metamorphism at 340 Ma (Rötzler & Romer, 2001). Another source already proposed could be an eclogite. From existing studies, the melt derived from such a rock would show very strong enrichment in Sr (Rapp, Watson, & Miller, 1991) and would be richer in Rb and Ba than Cs, which is the opposite to the trends observed in the KLA and RUB MIs (Figure 10). It is unlikely that the melt originated from a gabbro or basalt because otherwise it would have a positive Eu, Sr, and Ba anomaly due to the consumption of plagioclase during the melting reaction (Becker, 1996). The most likely candidates for the source of the melt are deeply subducted metasediments, possibly resembling the younger (336 Ma; Massonne, Kennedy, Nasdala, & Theye, 2007) diamond-bearing phengite gneisses and phengite-bearing HP granulites of the Erzgebirge (Kröner & Willner, 1998; Massonne & Fockenberg, 2012; Schmädicke, Okrusch, & Schmidt, 1992; Stöckhert, Trepmann, & Massone, 2009) where melt was recently identified in inclusions in garnet (Acosta-Vigil et al., 2017).

6.1.1 | A formation model for the melt-bearing eclogites

The source of RUB and KLA granitic melt is crustal and must be located in the subduction zone. During subduction, the slab and the mantle wedge are in contact and fluid or melt released from the slab can be transferred to the mantle wedge causing metasomatism (Condamine, Médard, & Devidal, 2016; Fumagalli, Zanchetta, & Poli, 2009; Scambelluri, Hermann, Morten, & Rampone, 2006). A similar genetic process may be envisioned for the ultramafic bodies here investigated, where a melt produced via melting of subducted crust migrates to the mantle wedge and causes a metasomatic interaction with an already inhomogeneous peridotite (Figure 12a, see also Section 6.5 for the KLA and RUB peridotite chemical features). Then portions of the metasomatized mantle wedge are incorporated in the underlying slab via ductile flow (Figure 12b), as proposed by Brueckner (1998) to explain the juxtaposition of garnet peridotites and continental crust. This scenario is based on the consideration that slab and mantle wedge are gravitationally unstable because of their strong difference in density, considerably higher in the overlying mantle wedge. If the slab at depth becomes hotter and/or wet (the latter possibly because of fluid/melt influx), the peridotite can sink as blobs in the crust, thus sharing afterwards their further evolution with the surrounding subducted crust (Figure 12c).

How the metasomatic melt migrates from the subducting slab into the mantle and how it interacts therein is a complex problem. The two processes proposed for magma migration are porous flow through the grain boundaries and flow through a fracture network (Schiano, Provost, Clocchiatti, & Faure, 2006). The first process would be more likely to promote an extensive interaction between melt and peridotite than the second, thus causing the melt to change its original composition. In the RUB and KLA case study, the melt chemistry suggests that there was no interaction with the peridotite during the migration and before its entrapment as inclusions in the garnet. The melt is indeed poor in MgO, Ni, and Cr (Table 1), whereas high-SiO_2 adakite magmas that interact with the mantle wedge peridotite during ascent show high concentrations of such elements (Martin et al., 2005). In addition, no evidences of peridotite–melt interaction are visible in the field, such as a network of veins in the peridotites around the pyroxenite lenses/layers described here, which may be considered indicative of pervasive flow. Therefore, the melt migration process occurred probably via channelized, maybe even fast-travelling flow (as proposed by Vrijmoed et al., 2013), which prevented the melt from interacting with the peridotite and thus preserved its pristine nature. Evidence of these channels was then erased by subsequent deformation and retrogression of the host peridotite after incorporation in the crust.

6.2 | The host rock: A mantle eclogite with crustal, subduction-related signature

Although previous works described the investigated rocks as garnet clinopyroxenites, in the present study the term 'eclogite' has been chosen to describe them because the newly acquired data set shows that both major element and mineral compositions of RUB and KLA samples are closer to eclogites, especially the Nové Dvory kyanite eclogites, rather than to pyroxenites of the Moldanubian zone (cf. Medaris, Beard, & Jelínek, 2006 and Figure 7). Furthermore, eclogite and pyroxenite of the Moldanubian Zone have been discriminated according to several parameters reported in Table 4 such as Na_2O, TiO_2 versus Cr and Ni, Mg#, and the Jd content in clinopyroxene (Carswell, 1990; Gonzaga et al., 2010; Medaris et al., 1995, 2006; Obata et al., 2006; Svojtka et al., 2016). All these parameters in RUB and KLA samples are consistent with an eclogite rather than a pyroxenite. The investigated rocks contain Na_2O ≥2 wt%, whereas pyroxenites contain generally Na_2O ≤1 wt% (0.7 wt% is the average in the Moldanubian Zone pyroxenites; Svojtka et al., 2016). Significantly, the TiO_2 content in samples RUB and KLA is higher than in the Moldanubian pyroxenites, whereas Cr and Ni contents are lower, again a feature of eclogites. A typical Moldanubian pyroxenite contains TiO_2 <0.3 wt%, Cr_2O_3 and Ni >400 ppm in average. Pyroxenite Mg# is generally >80, whereas for eclogite, and for RUB and KLA, it is lower. Clinopyroxene in RUB and KLA samples has a Jd content of 19–28 mol.%, that is, it is an omphacite (Jd ≥ 20–25 mol.%), as commonly observed in eclogite. By contrast, pyroxenite clinopyroxene is commonly augite–diopside or Cr-diopside.

The investigated eclogites have features more compatible with the oceanic crust than with the mantle peridotites and pyroxenites, notably the low Cr, Ni contents, and Mg#, despite being enclosed in mantle rocks. The major element contents are indeed generally very similar to N-MORB, that is, oceanic crust. For example, Na_2O generally fits in the range of common lower oceanic crust (2.23–3.27 wt%; Coogan, 2014). However, since MgO is lower than in N- and E-MORB, KLA and RUB samples display a typical Fe-rich basaltic composition. Such MgO values are in the range of low-MgO mantle garnet pyroxenite when compared with the database of Isabel Varas-Reus, Garrido, Marchesi, Bosch, and Hidas (2018), and their Mg# is the lowest with respect to the other pyroxenites and kyanite eclogite of the Moldanubian Zone. By contrast, Al_2O_3 content is rather high, in the range of high-Al_2O_3 mantle garnet pyroxenite (Isabel Varas-Reus et al., 2018). Consistent with the Fe-rich nature of the rocks, clinopyroxene and garnet are generally more Fe-rich than in the equivalent phases in the other pyroxenites. This feature suggests a protolith derived from, or related to, the oceanic crust.

The RUB and KLA samples also show a clear subduction-related trace element signature indicated by enrichment in LILE, positive U anomaly, and negative anomalies in Sr and Nb (Figure 8; Becker, 1996; Becker, Shirey, & Carlson, 2001; Medaris et al., 2015; Prouteau, Scaillet, & Pichavant, 2001; Zanetti, Mazzucchelli, Rivalenti, & Vannucci, 1999). In particular, the enrichment in Cs, Rb, Li, and LREEs observed in clinopyroxene is regarded as a monitor of metasomatism in mantle rock: Li in particular is a sensitive tracer of the slab-to-mantle transfer of fluids (Scambelluri et al., 2006 and references therein). Such a subduction-related signature is clearly due to the presence of melt during the crystallization of all the eclogite samples here investigated (RUB, KLA1, and KLA2) despite the slight difference in composition of the host garnet (see Figure 7).

6.3 | MI preserve the original metasomatic agent

In the present study, it is proposed that the melt trapped in the inclusions is of crustal origin (i.e. deeply subducted continental crust), externally derived with respect to the peridotite–pyroxenite–eclogite association, and has acted as a metasomatic agent during the crystallization of the eclogites.

This is the first case in which the metasomatic agent—a silicate melt—present at depth within an orogenic peridotite has been directly characterized.

Mantle metasomatism by subduction-related melts/fluids has already been extensively studied in several localities worldwide. The main features of metasomatized mantle rocks are whole-rock enrichment in K, Rb, Ba, Sr, and LREEs with respect to HREEs and, in case of a modal metasomatism, the crystallization of phlogopite, amphibole, and/or orthopyroxene (Becker, 1996; Becker et al., 2001; Prouteau et al., 2001; Rampone & Morten, 2001; Scambelluri et al., 2006; Schiano et al., 1995; Zanetti et al., 1999; Zhang et al., 2007; Zhang et al., 2011). In most of these case studies the composition of the metasomatic agent was inferred from the geochemical signature of bulk rock and/or minerals (Becker, 1996; Becker et al., 2001; Zanetti et al., 1999; Zhang et al., 2007) and only in a few cases was it possible to study directly the metasomatic agent (Schiano et al., 1995) or the remnants of it (Malaspina et al., 2006, 2009). The differences between RUB and KLA MI and the multiphase fluid inclusions described by Malaspina et al. (2006, 2009) are reflected in the mineral assemblages and the result of re-homogenization experiments (see discussion in Borghini et al., 2018).

Melt interpreted as a preserved metasomatic agent in glassy inclusions from spinel-bearing harzburgite xenoliths was reported by Schiano et al. (1995) in arc lavas from the Philippines. There the inclusions occur as trails in the porphyroclasts and isolated in metasomatic minerals, olivine, and orthopyroxene. They are either completely glassy ($\pm H_2O \pm$ sulphide) or glassy with daughter minerals such as phlogopite, amphibole, orthopyroxene, and clinopyroxene. The reported melt composition is different from the one investigated in this study: SiO_2 content and the alkalis (Na_2O and K_2O) are higher in RUB and KLA MIs, whereas TiO_2, FeO, P_2O_5 and CaO are higher in the Philippine examples (see composition in Table 1). Moreover, sulphides are absent in both Granulitgebirge samples. Schiano et al. (1995) suggested that the melt originated via a small degree of partial melting of the oceanic crust at the garnet–amphibolite/eclogite transition, with garnet, hornblende, and clinopyroxene as residual phases. The newly studied eclogites are, however, different for several reasons: the melt has a different composition; the glass inclusions do not show water shrinkage bubbles and/or sulphides; and the daughter phases are mostly anhydrous and fill the whole inclusion (Figures 4 and 5). Also, there are no clear residual phases: both garnet and clinopyroxene are instead interpreted as the products of reaction at the metamorphic peak. The participation of melt in this process is usually via a peritectic reaction in which a liquid reacts with a solid (in this case a still undefined mafic layer in the mantle; see Section 6.4 for details) and gives, as a result, other solids without changing its composition. That the melt did not change in composition during the growth of the host garnet is testified by the fact that the primary inclusions show the same composition across the whole garnet, which is moreover not zoned. Alternatively, the melt could just as easily have acted as a kinetic agent, enhancing rapid crystallization of the peak phases, enriching them in specific trace elements but without contributing to their major element chemistry, and locally becoming trapped in the growing garnet.

6.3.1 | Same metasomatic signature, different rocks

Remarkably, other rocks in the Bohemian Massif show geochemical signatures requiring a component very close to that of the melt hosted in the investigated eclogites. For instance, unusual melanosyenites in the Bohemian Massif—the so-called durbachite suite—show chemical features similar to the melt trace element pattern, that is, high LILE (higher Cs than Rb and Ba) and LREEs, U, Th, and strong Pb-positive anomaly and Nb- and Ti-negative anomaly (Figure 10; Janoušek & Holub, 2007). The durbachite suite has been interpreted as being derived from an anomalous mantle source contaminated by mature crustal material (Janoušek & Holub, 2007), like other potassic mafic magmas that were emplaced throughout the Variscan belt at the same time (Couzinié et al., 2016; von Raumer, Finger, Veselá, & Stampfli, 2014). In this scenario, a melt similar to the one trapped in the eclogites reported here may represent the crustal component added to the source of such magmas, an occurrence which requires both melts to have been produced by similar source rocks under similar fluid-present conditions.

A melt very similar to the one hosted in KLA and RUB eclogites was most likely also the agent of the reported cryptic metasomatism in garnet peridotite with lenses of phlogopite-garnet pyroxenite in the T-7 borehole in the Saxothuringian Zone (Medaris et al., 2015; Figure 10). These peridotites experienced two types of metasomatisms: modal, materialized by the occurrence of phlogopite and small amounts of amphibole, and cryptic, visible as trace element enrichment. The metasomatic agent was interpreted by Medaris et al. (2015) to be subduction zone-related. The trace element patterns of the T-7 peridotites strongly resemble the melt in RUB and KLA MI, in particular, in terms of positive anomalies for Th, U, and Pb, negative anomalies for Nb, Ta, Sr, and Ti strongly supporting the same kind of metasomatic history in all of these widely spaced garnet–clinopyroxene rocks.

6.4 | A conundrum: Eclogites with preserved metasomatic agent and no metasomatic signature

The detailed geochemical investigation of these eclogites and the trapped melt reveals a very puzzling feature: while some

key elements enriched in the bulk rock can be attributed to the presence of melt and both garnet and clinopyroxene are to different degrees enriched in incompatible elements, the overall bulk rock trace element pattern of the eclogite does not register the presence of the metasomatic melt, despite the melt being present inside the rock as inclusions.

In terms of modal metasomatism, 'classic' metasomatic phases, for example, phlogopite, amphibole±apatite, are notably absent from the metamorphic peak assemblage, consistently with the dry character of both main phases (garnet and clinopyroxene). As already made clear in the petrographic descriptions, these 'classic' metasomatic phases are present in the matrix together with leucocratic pockets filled with plagioclase (Figure 3e,f) but these represent a later modal metasomatism that post-dates the metamorphic peak and is unrelated to the preserved MI. Leucocratic pockets have been already reported in the Nové Dvory eclogite where they contain plagioclase, a moderate amount of garnet, clinopyroxene and minor biotite and amphibole (Miyazaki et al., 2016). Clinopyroxene in the latter has been interpreted as having crystallized from a melt with composition close to a high-pressure TTG. The melt pockets in RUB and KLA eclogites, however, only contain plagioclase, whereas the clinopyroxene belongs to the peak assemblage. Furthermore, the metasomatism of a peridotite by a granitic/granitoid melt is expected to cause abundant crystallization of orthopyroxene with the consequent formation of an Ol-free garnet pyroxenite (Rampone & Morten, 2001). Even aqueous fluids of eclogitic origin can crystalize orthopyroxene in mantle rocks as demonstrated by natural examples (Malaspina et al., 2017), thermodynamic/mass balance studies (Campione, Tumiati, & Malaspina, 2017) and experimental works (Tiraboschi et al., 2018). RUB and KLA garnet clinopyroxene-rich rocks are orthopyroxene-free, and the production of garnet and clinopyroxene requires a high amount of CaO, an element which is instead not abundant: neither in the melt (CaO in the melt <1 wt%; see Table 1) nor in Rubinberg and Klatschmühle peridotite (Schmädicke et al., 2010). This suggests that either a Ca-rich rock layer, such as a gabbro, was already present in the peridotite, or there was another component involved in peak metamorphism, now totally consumed, that is, a CaO- and FeO-rich melt or fluid. The first scenario is more plausible and, either way, the presence of abundant CaO in the system explains the crystallization of clinopyroxene rather than orthopyroxene.

In terms of cryptic metasomatism, the major elements in the eclogite bulk rock analyses, and some of the trace elements, especially Cs and U, are consistent with a crustal- and subduction-related signature. A first reasonable inference is that the trapped melt, originating in the crust, should be responsible for such a signature. However, when melt and bulk rock trace elements are compared they appear notably different insofar as that only Cs shows the same degree of enrichment in both, and that most of the normalized patterns are instead rather flat, as expected for an unmetasomatized mantle (Figure 8). As previously discussed, metasomatized peridotites and pyroxenites from the T-7 borehole (Medaris et al., 2015) show instead a signature very similar to the melt trapped in the Granulitgebirge eclogites, despite the apparent absence of MIs (Figure 10).

The conundrum of the absence of a metasomatic footprint in rocks containing a metasomatic melt could be solved by taking into account the size of the melt remnants. Despite the fact that MI are abundant in the RUB and KLA eclogites, the overall amount of melt still present in the rock is extremely small, due to the micrometric size of the inclusions, and thus not sufficient to dominate the whole-rock signature. Such a minor amount of trace elements enrichment may thus be a direct expression of the limited amount of melt present during peak metamorphism of the eclogites: something also consistent with the absence of classic hydrous metasomatic phases in the peak assemblage. On the other hand, rocks in the T-7 borehole would have experienced a larger influx of melt thus recrystallizing extensively with the formation of classic metasomatic phases. According to our hypothesis the two rocks (the investigated eclogites and the mantle rocks from the T-7 borehole) experienced different degrees of metasomatism caused by the infiltration of a similar metasomatic agent, now preserved in the less metasomatized of the two. Clinopyroxene in the Granulitgebirge eclogites seems to be the only peak phase recording the interaction with the melt as it shows enrichment in Rb, Cs, U, and Li, and possibly LREEs even though it is devoid of MIs. Clinopyroxene can trap inclusions (e.g. Salvioli-Mariani, Mattioli, Renzulli, & Serri, 2002; Schiano, Clocchiatti, Boivin, & Medard, 2004; Veksler, Nielsen, & Sokolov, 1998) and their absence can be explained by recrystallization of the clinopyroxene to smaller sized grains, which caused the obliteration of the inclusions. This is also supported by the size difference between garnet, generally larger, and clinopyroxene (see Figure 3c,d).

6.5 | Peculiar melt-bearing eclogites versus other pyroxenites/eclogites of the Bohemian Massif

Mantle-derived garnet clinopyroxenites and associated rocks (eclogites, websterites, garnetites, etc.,) have been studied mainly from xenoliths worldwide but the Bohemian Massif, where numerous orogenic garnet- and spinel-bearing peridotite bodies with enclosed pyroxenites and eclogite are exposed, has presented a fantastic opportunity to study a wide variety of such rocks in situ. The formation of the lenses and layers of pyroxenite has been explained by a variety of processes: HP crystal segregation from basaltic melts of different origins; peridotite metasomatism; HP recrystallization of

basalts/gabbros; and stress-induced recrystallization of megacrysts. How can the textures, major and trace element data of whole rock, minerals, and MI in the newly studied RUB and KLA samples be explained in terms of these different garnet clinopyroxenite and eclogite types?

The most known and best-characterized pyroxenites of the Granulitgebirge are those from Reinsdorf (also called Gilsberg), 10 km west of where samples RUB and KLA were collected (Massonne & Bautsch, 2002; Schmädicke et al., 2010). Reinsdorf pyroxenites are very different from the garnet+clinopyroxene-rich rocks studied here from both microstructural and geochemical viewpoints. The main microstructural difference is the presence in Reinsdorf samples of alternating parallel lamellae of garnet (the minor component) in clinopyroxene (the major phase) surrounded by a recrystallized equigranular garnet+clinopyroxene domain. Clearly, these rocks were originally layers of aluminous, pyroxene megacrysts, which experienced deformation-induced exsolution of garnet and recrystallization at higher pressure (Massonne & Bautsch, 2002). Geochemically, garnet, clinopyroxene, and bulk rock all show similar REE trends. Clinopyroxene is richer in LREEs and garnet enriched in HREEs, but Ce, Pr, and Nd are depleted in both minerals as well as in the bulk rock. In comparison, RUB and KLA eclogites have very different textures and show no evidence of exsolution. Also, as garnet preserves clusters of primary MI its growth took place in the presence of melt rather as a result of exsolution- or deformation-induced, solid-state recrystallization, as reported from Reinsdorf. Elsewhere in the Bohemian Massif there are several locations where rocks similar to those of Reinsdorf have been reported, for example, Horní Bory, Biskupice, Nové Dvory, Kutná Hora, Křemže (Czech Republic), Karlstetten and Meidling im Tal (Lower Austria), all belonging to the Moldanubian Zone. Here also other varieties of pyroxenites occur and they can be grouped in the three types, Mohelno, Horní Bory, and Nové Dvory (Medaris et al., 2005; see locations in Figure 1). Precisely those pyroxenites and kyanite eclogite types from the three named localities have been chosen for the comparison with RUB and KLA samples (Figure 7; see Sections 6.1 and 6.2). In terms of the whole-rock major elements data, RUB and KLA samples are very similar, except for a slightly higher TiO_2 and FeO and lower CaO content, when compared with the kyanite eclogite from Nové Dvory: a rock quite different from all the other Moldanubian pyroxenites (Obata et al., 2006; Figure 7; Table 1). The comparison of the whole-rock trace element patterns shows some peculiar features of RUB and KLA samples: LILE enrichment and positive U and Ti anomalies. The slightly negative Pb anomaly of RUB and KLA specimens contrasts with a positive Pb anomaly in the Moldanubian samples (Figure 8a). The LREE enrichment in both RUB and KLA analyses is higher than in the whole Moldanubian data set, whereas the comparison of HREEs

shows higher abundances in RUB but slightly lower values in KLA (Figure 8b). Garnet and clinopyroxene trace element patterns show also that RUB and KLA samples are generally enriched with respect to the Moldanubian ones (Figure 9). Moreover, the clinopyroxene patterns with high LILE, Th, Li and B content, negative Pb anomaly, and REE convex upward pattern, are in strong contrast with those of the Mohelno type that are richer in HREEs due to the absence of garnet (Figure 9b and d). In fact, Mohelno-type pyroxenites are spinel- and orthopyroxene-bearing (Figure 9d). The three Moldanubian pyroxenite types occur in peridotites attributed to three different mantle environments (Medaris, Beard, & Jelínek, 2006; Medaris et al., 2005): suboceanic asthenospheric mantle for the Mohelno type, disrupted mafic–ultramafic cumulate complex for Horní Bory, and subcontinental lithospheric mantle for Nové Dvory type. The proposed genesis for those pyroxenites is either as HP cumulates (Svojtka et al., 2016) or due to HP recrystallization of gabbroic cumulates (Obata et al., 2006; Svojtka et al., 2016). The important geochemical differences discussed here suggest then a different genetic process for RUB and KLA samples.

6.5.1 | Eclogite and peridotite with multiphase solid inclusions of the Bohemian Massif

Some of the Bohemian Massif eclogites and peridotites contain multiphase solid inclusions (MSIs) that can be compared with the ones investigated in the present paper. MSIs were reported in eclogite from Nové Dvory (Faryad, Jedlicka, & Ettinger, 2013) but, with respect to the RUB and KLA nanogranitoids, they contain different modal amounts of phases, different assemblages and thus variable composition. The inclusions in the Nové Dvory eclogites have been interpreted as the result of post-entrapment decomposition of former hydrous minerals included in garnet while it was growing, rather than melt trapped in the garnet. The presence of primary MI and the peculiar trace elements patterns in bulk rock, garnet, and clinopyroxene suggest a different genesis for RUB and KLA eclogite with respect to the Nové Dvory equivalents, even though they both form layers in Variscan mantle peridotites. Interestingly, some eclogites from Dunkelsteinerwald (Austrian part of the Bohemian Massif) show MSIs with aspect and phase assemblage very close to a nanogranitoid (Ferrero, O'Brien, et al., 2018; see fig. 2d in Faryad et al., 2013) but interpreted by Faryad et al., 2013, in the same way as for the Nové Dvory examples.

Another location where MSIs have been reported in orogenic garnet peridotite is Plešovice in the Blanský Les Massif, South Bohemia (Naemura, Hirajima, Svojtka, Shimizu, & Iizuka, 2018). Here, the inclusions occur in Zn-poor chromite, have a negative crystal shape and contain mainly hydrous

aluminosilicate minerals (phlogopite), phosphates (mainly apatite), and carbonates (calcite and dolomite). The melt composition has been calculated using the mineral proportions and mineral compositions and corresponds to a carbonated potassic silicate melt. This composition is very different from the melt observed in the Rubinberg and Klatschmühle eclogites, although the trace element enrichment patterns, for example, positive Th and negative Sr and Ti anomalies in the garnet, are comparable.

Finally, some garnet peridotite from the T-7 borehole, Saxothuringian Zone, contains negative crystal-shaped MSIs in garnet annuli (Čopjaková & Kotková, 2018). The mineral assemblage of these MSIs is, however, very different from the one reported for RUB and KLA samples, insofar as they contain in variable proportions: barian mica, amphibole, magnesite, and dolomite±other accessory phases. Such MSIs have been interpreted, based on the chemical composition on the barian mica alone, as the result of the metasomatism of the mantle wedge via a crustal-derived subduction-related fluid.

7 | CONCLUSIONS

The eclogites (formerly called pyroxenites) of Rubinberg and Klatschmühle enclosed in the peridotites of the Granulitgebirge contain inclusions of granitic melt occurring as nanogranitoids, a peculiar feature that makes them unique among the pyroxenite/eclogite bodies in orogenic peridotites worldwide. In the present study, we report the first detailed geochemical and microstructural study of the eclogite lenses and a metasomatic agent present during subduction in the Variscan orogeny. The melt is granitic, peraluminous, hydrous, and enriched in Cs, Li, B, Pb, Rb, and Ba, all elements typical of the continental crust. Since such a melt cannot be a product of mantle melting, it is interpreted as the preserved metasomatic agent now stored in inclusions in garnet. This preserved melt is the one that originally infiltrated the rock, and acted as a kinetic agent inducing garnet and clinopyroxene crystallization without contributing to the major element chemistry but just to the enrichment of some specific trace elements.

The host eclogite compositions are close to that of a Fe-rich basalt and the high amounts of Cs and U are also consistent with a subduction-related signature. These different signatures imply that the eclogites formed due to metasomatic interaction between mafic/ultramafic layers in mantle peridotite and a melt produced via partial melting of the deeply subducted continental crust. In fact, the low Mg and high Ca and Fe contents in eclogite can be most likely explained by the presence in the peridotite of a Ca-rich rock layer now totally consumed, as the preserved melt is not enriched in any of these components.

The trapped melt shows a close resemblance in trace elements with the components of the pattern of the durbachite suite attributed to a mature crustal component, thus suggesting that a melt very similar to the one enclosed in the eclogite was involved in durbachite formation. Some of the elements—Th, U, Pb, Nb, Ta, and Ti—in RUB and KLA melt patterns show analogue trends also to the ones in the bulk rock of the peridotite and pyroxenite in the T-7 borehole, suggesting that an akin melt was their metasomatic agent.

Despite the presence of MI entrapped in the garnet the evidence of metasomatism in the eclogites, both modal and cryptic, is limited. By contrast, the metasomatized peridotite and pyroxenite of the T-7 borehole register the melt signature. This discrepancy can be explained with a different degree of metasomatism, with Granulitgebirge rocks experiencing a more limited influx of the melt, not sufficient to impose its signature. The comparison with other pyroxenites and eclogites of the Bohemian Massif shows some similarities only in terms of major elements with the Nové Dvory kyanite eclogite, whereas the trace elements are very different.

ORCID

Alessia Borghini 🄳 https://orcid.org/0000-0002-0857-627X

REFERENCES

Acosta-Vigil, A., Buick, I., Hermann, J., Cesare, B., Rubatto, D., London, D., & Morgan, G. B. (2010). Mechanisms of crustal anatexis: A geochemical study of partially melted metapelitic enclaves and host dacite, SE Spain. *Journal of Petrology*, *51*(4), 785–821. https://doi.org/10.1093/petrology/egp095

Acosta-Vigil, A., Stöckhert, B., Hermann, J., Yaxley, G., Cesare, B., & Bartoli, O. (2017). Remelting of nanogranitoids in UHP felsic granulites from Erzgebirge (Bohemian Massif, Germany). American Geophysical Union, Fall Meeting 2017, Abstract #V24B-06 (December 2017).

Allègre, C. J., & Turcotte, D. L. (1986). Implications of a two-component marble-cake mantle. *Nature*, *323*, 123–127. https://doi.org/10.1038/323123a0

Becker, H. (1996). Crustal trace element and isotopic signatures in garnet pyroxenites from garnet peridotite massifs from Lower Austria. *Journal of Petrology*, *37*(4), 272–286. https://doi.org/10.1093/petrology/37.4.785

Becker, H., Shirey, S. B., & Carlson, R. W. (2001). Effects of melt percolation on the Re-Os systematics of periodites from a Paleozoic convergent plate margin. *Earth and Planetary Science Letters*, *188*(1–2), 107–121. https://doi.org/10.1016/S0012-821X(01)00308-9

Bodinier, J.-L., & Godard, M. (2014). Orogenic, ophiolitic, and abyssal peridotites. Treatise on Geochemistry: Second Edition (3rd ed., Vol. 3). Elsevier. https://doi.org/10.1016/B978-0-08-095975-7.00204-7

Bodinier, J.-L., Guiraud, M., Fabriès, J., Dostal, J., & Dupuy, C. (1987). Petrogenesis of layered pyroxenites from the Lherz, Freychinède and Prades ultramafic bodies (Ariège, French Pyrénées). *Geochimica et Cosmochimica Acta*, *51*, 279–290.

Borghini, A., Ferrero, S., Wunder, B., Laurent, O., O'Brien, P. J., & Ziemann, M. A. (2018). Granitoid melt inclusions in orogenic peridotite and the origin of garnet clinopyroxenite. *Geology*, *46*(11), 1007–1010. https://doi.org/10.1130/G45316.1

Brueckner, H. K. (1998). Sinking intrusion model for the emplacement of garnet-bearing peridotites into continent collision orogens. *Geology*, *26*(7), 631–634. https://doi.org/10.1130/0091-7613(1998)026<0631:SIMFTE>2.3.CO;2

Brueckner, H. K., & Medaris, L. G. (2000). A general model for the intrusion and evolution of "mantle" garnet peridotites in high-pressure and ultra-high-pressure metamorphic terranes. *Journal of Metamorphic Geology*, *18*, 123–133. https://doi.org/10.1046/j.1525-1314.2000.00250.x

Campione, M., Tumiati, S., & Malaspina, N. (2017). Primary spinel + chlorite inclusions in mantle garnet formed at ultrahigh-pressure. *Geochemical Perspectives Letters*, *4*, 19–23. https://doi.org/10.7185/geochemlet.1730.

Carswell, D. A. (1990). Eclogites and the eclogite facies: Definitions and classifications. In D. A. Carswell (Ed.), *Eclogite facies rocks*. Blackie/Springer: Glasgow, UK and London, UK.

Carswell, D. A., & Jamtveit, B. (1990). Variscan Sm-Nd ages for the high-pressure metamorphism in the Moldanubian Zone of the Bohemian Massif, Lower Austria. *Neues Jahrbuch Für Mineralogie-Abhandlungen*, *162*(1), 69–78.

Carswell, D. A., & O'Brien, P. J. (1993). Thermobarometry and geotectonic significance of high-pressure granulites: Examples from the moldanubian zone of the Bohemian Massif in lower Austria. *Journal of Petrology*, *34*(3), 427–459. https://doi.org/10.1093/petrology/34.3.427

Cesare, B., Acosta-Vigil, A., Bartoli, O., & Ferrero, S. (2015). What can we learn from melt inclusions in migmatites and granulites? *Lithos*, *239*, 186–216. https://doi.org/10.1016/j.lithos.2015.09.028

Condamine, P., Médard, E., & Devidal, J. L. (2016). Experimental melting of phlogopite-peridotite in the garnet stability field. *Contributions to Mineralogy and Petrology*, *171*(11), 1–26. https://doi.org/10.1007/s00410-016-1306-0

Coogan, L. A. (2014). The lower oceanic crust. In R. L. Rudnick (Ed.), *The crust*. Treatise on Geochemistry (second edition) (vol. 4, pp. 497–541). Elsevier.

Cooke, R. A., & O'Brien, P. J. (2001). Resolving the relationship between high P-T rocks and gneisses in collisional terranes: An example from the Gföhl gneiss-granulite association in the Moldanubian Zone, Austria. *Lithos*, *58*(1–2), 33–54. https://doi.org/10.1016/S0024-4937(01)00049-4

Čopjaková, R., & Kotková, J. (2018). Composition of barian mica in multiphase solid inclusions from orogenic garnet peridotites as evidence of mantle metasomatism in a subduction zone setting. *Contributions to Mineralogy and Petrology*, *173*(12), 1–18. https://doi.org/10.1007/s00410-018-1534-6.

Couzinié, S., Laurent, O., Moyen, J. F., Zeh, A., Bouilhol, P., & Villaros, A. (2016). Post-collisional magmatism: Crustal growth not identified by zircon Hf–O isotopes. *Earth and Planetary Science Letters*, *456*(1), 182–195. https://doi.org/10.1016/j.epsl.2016.09.033

Faryad, S. W., Dolejš, D., & Machek, M. (2009). Garnet exsolution in pyroxene from clinopyroxenites in the Moldanubian zone: Constraining the early pre-convergence history of ultramafic rocks in the Variscan orogen. *Journal of Metamorphic Geology*, *27*(9), 655–671. https://doi.org/10.1111/j.1525-1314.2009.00834.x

Faryad, S. W., Jedlicka, R., & Ettinger, K. (2013). Subduction of lithospheric upper mantle recorded by solid phase inclusions and compositional zoning in garnet: Example from the Bohemian Massif. *Gondwana Research*, *23*(3), 944–955. https://doi.org/10.1016/j.gr.2012.05.014

Ferrero, S., & Angel, R. J. (2018). Micropetrology: Are inclusions grains of truth? *Journal of Petrology*, *59*(9), 1671–1700. https://doi.org/10.1093/petrology/egy075

Ferrero, S., Godard, G., Palmieri, R., Wunder, B., & Cesare, B. (2018). Partial melting of ultramafic granulites from Dronning Maud Land, Antarctica: Constraints from melt inclusions and thermodynamic modeling. *American Mineralogist*, *103*(4), 610–622. https://doi.org/10.2138/am-2018-6214

Ferrero, S., O'Brien, P. J., Borghini, A., Wunder, B., Wälle, M., Günter, C., & Ziemann, M. A. (2018). A treasure chest full of nanogranitoids : An archive to investigate crustal melting in the Bohemian Massif. In S. Ferrero, P. Lanari, P. Goncalves, & E. G. Grosch (Eds.), *Metamorphic geology: Microscale to mountain Belts. Geological Society, London, Special Publication*, (Vol.*478*).

Ferrero, S., Wunder, B., Walczak, K., O'Brien, P. J., & Ziemann, M. A. (2015). Preserved near ultrahigh-pressure melt from continental crust subducted to mantle depths. *Geology*, *43*(5), 447–450. https://doi.org/10.1130/G36534.1

Ferrero, S., Ziemann, M. A., Angel, R. J., O'Brien, P. J., & Wunder, B. (2016). Kumdykolite, kokchetavite, and cristobalite crystallized in nanogranites from felsic granulites, Orlica-Snieznik Dome (Bohemian Massif): Not an evidence for ultrahigh-pressure conditions. *Contributions to Mineralogy and Petrology*, *171*(1), 1–12. https://doi.org/10.1007/s00410-015-1220-x

Franke, W. (1989). Tectonostratigraphic units in the Variscan belt of central Europe. *Geological Society of America Special Paper*, *230*, 67–90.

Franke, W. (2000). The mid-European segment of the Variscides: Tectonostratigraphic units, terrane boundaries and plate tectonic evolution. *Geological Society, London, Special Publications*, *179*(1), 35–61. https://doi.org/10.1144/gsl.sp.2000.179.01.05

Franke, W., & Żelaźniewicz, A. (2000). The eastern termination of the Variscides: Terrane correlation and kinematic evolution. *Geological Society, London, Special Publications*, *179*(1), 63–86. https://doi.org/10.1144/GSL.SP.2000.179.01.06

Frezzotti, M. L., Ferrando, S., Dallai, L., & Compagnoni, R. (2007). Intermediate alkali – Alumino-silicate aqueous aolutions released by deeply subducted continental crust: Fluid evolution in UHP OH-rich topaz – Kyanite quartzites from Donghai (Sulu, China). *Journal of Petrology*, *48*(6), 1219–1241. https://doi.org/10.1093/petrology/egm015

Fumagalli, P., Zanchetta, S., & Poli, S. (2009). Alkali in phlogopite and amphibole and their effects on phase relations in metasomatized peridotites: A high-pressure study. *Contributions to Mineralogy and Petrology*, *158*(6), 723–737. https://doi.org/10.1007/s00410-009-0407-4

Garrido, C. J., & Bodinier, J.-L. (1999). Diversity of mafic rocks in the Ronda peridotite: Evidence for pervasive melt-rock reaction during heating of subcontinental lithosphere by upwelling asthenosphere. *Journal of Petrology*, *40*(5), 729–754. https://doi.org/10.1093/petroj/40.5.729

Gonzaga, R. G., Lowry, D., Jacob, D. E., LeRoex, A., Schulze, D., & Menzies, M. A. (2010). Eclogites and garnet pyroxenites: Similarities and differences. *Journal of Volcanology and Geothermal Research*, *190*(1–2), 235–247. https://doi.org/10.1016/j.jvolgeores.2009.08.022

Guillong, M., Meier, D. L., Allan, M. M., Heinrich, C. A., & Yardley, B. W. D. (2008). SILLS: A Matlab-based program for the reduction of laser ablation ICP–MS data of homogeneous materials and inclusions. *Mineralogical Association of Canada Short Course*, *40*(June 2015), 328–333.

Hartmann, G., & Wedepohl, K. H. (1993). The composition of peridotite tectonites from the Ivrea Complex, northern Italy: Residues from melt extraction. *Geochimica et Cosmochimica Acta*, *57*, 1761–1782. https://doi.org/10.1016/0016-7037(93)90112-A

Hastie, A. R., Kerr, A. C., McDonald, I., Mitchell, S. F., Pearce, J. A., Wolstencroft, M., & Millar, I. L. (2010). Do cenozoic analogues support a plate tectonic origin for earth's earliest continental crust? *Geology*, *38*(6), 495–498. https://doi.org/10.1130/G30778.1

Hermann, J., & Rubatto, D. (2009). Accessory phase control on the trace element signature of sediment melts in subduction zones. *Chemical Geology*, *265*(3–4), 512–526. https://doi.org/10.1016/j.chemgeo.2009.05.018

Isabel Varas-Reus, M., Garrido, C. J., Marchesi, C., Bosch, D., & Hidas, K. (2018). Genesis of ultra-high pressure garnet pyroxenites in orogenic peridotites and its bearing on the compositional heterogeneity of the earth's mantle. *Geochimica and Cosmochimica Acta*, https://doi.org/10.1016/j.gca.2018.04.033

Janoušek, V., & Holub, F. V. (2007). The causal link between HP-HT metamorphism and ultrapotassic magmatism in collisional orogens: Case study from the Moldanubian Zone of the Bohemian Massif. *Proceedings of the Geologists' Association*, *118*(1), 75–86. doi:https://doi.org/10.1016/S0016-7878(07)80049-6.

Jochum, K. P., Weis, U., Stoll, B., Kuzmin, D., Yang, Q., Raczek, I., … Enzweiler, J. (2011). Determination of reference values for NIST SRM 610–617 glasses following ISO Guidelines. *Geostandards and Geoanalytical Research*, *35*, 397–429. https://doi.org/10.1111/j.1751-908X.2011.00120.x

Kotková, J., O'Brien, P. J., & Ziemann, M. A. (2011). Diamond and coesite discovered in Saxony-type granulite: Solution to the Variscan garnet peridotite enigma. *Geology*, *39*(7), 667–670. https://doi.org/10.1130/G31971.1

Kröner, A., Jaeckel, P., Reischmann, T., & Kroner, U. (1998). Further evidence for an early Carboniferous (~340 Ma) age of high-grade metamorphism in the Saxonian granulite complex. *Geologische Rundschau*, *86*(4), 751–766. https://doi.org/10.1007/PL00009939

Kröner, A., & Willner, A. P. (1998). Time of formation and peak of Variscan HP-HT metamorphism of quartz-feldspar rocks in the central Erzgebirge, Saxony, Germany. *Contributions to Mineralogy and Petrology*, *132*(1), 1–20. https://doi.org/10.1007/s004100050401

Malaspina, N., Hermann, J., & Scambelluri, M. (2009). Fluid/mineral interaction in UHP garnet peridotite. *Lithos*, *107*(1–2), 38–52. https://doi.org/10.1016/j.lithos.2008.07.006

Malaspina, N., Hermann, J., Scambelluri, M., & Compagnoni, R. (2006). Polyphase inclusions in garnet-orthopyroxenite (Dabie Shan, China) as monitors for metasomatism and fluid-related trace element transfer in subduction zone peridotite. *Earth and Planetary Science Letters*, *249*(3–4), 173–187. https://doi.org/10.1016/j.epsl.2006.07.017

Malaspina, N., Langenhorst, F., Tumiati, S., Campione, M., Frezzotti, M. L., & Poli, S. (2017). The redox budget of crust-derived fluid phases at the slab-mantle interface. *Geochemica et Cosmochimica Acta*, *209*, 70–84. https://doi.org/10.1016/j.gca.2017.04.004

Martin, H., Smithies, R. H., Rapp, R., Moyen, J. F., & Champion, D. (2005). An overview of adakite, tonalite-trondhjemiten-granodiorite (TTG), and sanukitoid: Relationships and some implications for crustal evolution. *Lithos*, *79*(1–2) Special Issue, 1–24. doi:https://doi.org/10.1016/j.lithos.2004.04.048.

Massonne, H.-J. (2001). First find of coesite in the ultrahigh-pressure metamorphic area of the central Erzgebirge, Germany. *European Journal of Mineralogy*, *13*(3), 565–570. https://doi.org/10.1127/0935-1221/2001/0013-0565

Massonne, H.-J., & Bautsch, H.-J. (2002). An unusual garnet pyroxenite from the Granulitgebirge, Germany: Origin in the transition zone (>400 km depths) or in a shallower upper mantle region? *International Geology Review*, *44*(9), 779–796. https://doi.org/10.2747/0020-6814.44.9.779

Massonne, H.-J., & Fockenberg, T. (2012). Melting of metasedimentary rocks at ultrahigh pressure—Insights from experiments and thermodynamic calculations. *Lithosphere*, *4*, 269–285. https://doi.org/10.1130/L185.1

Massonne, H.-J., Kennedy, A., Nasdala, L., & Theye, T. (2007). Dating of zircon and monazite from diamondiferous quartzofeldspathic rocks of the Saxonian Erzgebirge—Hints at burial and exhumation velocities. *Mineralogical Magazine*, *71*(4), 407–425. https://doi.org/10.1180/minmag.2007.071.4.407

Matte, P., Maluski, H., Rajlich, P., & Franke, W. (1990). Terrane boundaries in the Bohemian Massif: Result of large-scale Variscan shearing. *Tectonophysics*, *177*(1–3), 151–170. https://doi.org/10.1016/0040-1951(90)90279-H

McDonough, W. F., Sun, S.-S. (1995). The composition of the Earth. *Chemical Geology*, *120*, 223–253. https://doi.org/10.1016/0009-2541(94)00140-4

Medaris, L. G., Ackerman, L., Jelínek, E., Michels, Z. D., Erban, V., & Kotková, J. (2015). Depletion, cryptic metasomatism, and modal metasomatism (refertilization) of Variscan lithospheric mantle: Evidence from major elements, trace elements, and Sr-Nd-Os isotopes in a Saxothuringian garnet peridotite. *Lithos*, *226*(May), 81–97. https://doi.org/10.1016/j.lithos.2014.10.007

Medaris, L. G., Beard, B. L., & Jelínek, E. (2006). Mantle-derived, UHP garnet pyroxenite and eclogite in the Moldanubian Gföhl Nappe, Bohemian Massif: A geochemical review, new P-T determinations, and tectonic interpretation. *International Geology Review*, *48*(9), 765–777. https://doi.org/10.2747/0020-6814.48.9.765

Medaris, L. G., Beard, B. L., Johnson, C. M., Valley, J. W., Spicuzza, M. J., Jelínek, E., & Mísâr, Z. (1995). Garnet pyroxenite and eclogite in the Bohemian Massif: Geochemical evidence for Variscan recycling of subducted lithosphere. *Geologische Rundschau*, *84*(3), 489–505. https://doi.org/10.1007/BF00284516

Medaris, L. G., & Carswell, D. A. (1990). Petrogenesis of Mg-Cr garnet peridotites in European metamorphic belts. In D. A. Carswell (Ed.), *Eclogite facies rocks*. Blackie/Chapman and Hall: Glasgow, UK and London, UK.

Medaris, L. G., Wang, H., Jelínek, E., Mihaljevič, M., & Jakeš, P. (2005). Characteristics and origins of diverse Variscan peridotites in the Gföhl Nappe, Bohemian Massif, Czech Republic. *Lithos*, *82*(1–2) Special Issue, 1–23. doi:https://doi.org/10.1016/j.lithos.2004.12.004.

Miyazaki, T., Nakamura, D., Tamura, A., Svojtka, M., Arai, S., & Hirajima, T. (2016). Evidence for partial melting of eclogite from the Moldanubian Zone of the Bohemian Massif, Czech Republic. *Journal of Mineralogical and Petrological Sciences*, *111*(6), 405–419. https://doi.org/10.2465/jmps.151029c

Morgan, G. B., & London, D. (2005). Effect of current density on the electron microprobe analysis of alkali aluminosilicate glasses. *American Mineralogist*, *90*(7), 1131–1138. https://doi.org/10.2138/am.2005.1769

Naemura, K., Hirajima, T., Svojtka, M., Shimizu, I., & Iizuka, T. (2018). Fossilized melts in mantle wedge peridotites. *Scientific Reports*, *8*(1), 1–12. https://doi.org/10.1038/s41598-018-28264-6

Nasdala, L., & Massonne, H.-J. (2000). Microdiamonds from the Saxonian Erzgebirge, Germany: In situ micro-Raman characterisation. *European Journal of Mineralogy*, *12*(2), 495–498. https://doi.org/10.1127/0935-1221/2000/0012-0495

O'Brien, P. J. (2000). The fundamental Variscan problem: High-temperature metamorphism at different depths and high-pressure metamorphism at different temperatures. *Geological Society, London, Special Publications*, *179*(1), 369–386. https://doi.org/10.1144/GSL.SP.2000.179.01.22

O'Brien, P. J. (2006). Type-locality granulites: High-pressure rocks formed at eclogite-facies conditions. *Mineralogy and Petrology*, *86*(3–4), 161–175. https://doi.org/10.1007/s00710-005-0108-2

O'Brien, P. J. (2008). Challenges in high-pressure granulite metamorphism in the era of pseudosections: Reaction textures, compositional zoning and tectonic interpretation with examples from the Bohemian Massif. *Journal of Metamorphic Geology*, *26*(2), 235–251. https://doi.org/10.1111/j.1525-1314.2007.00758.x

O'Brien, P. J., & Carswell, D. A. (1993). Tectonometamorphic evolution of the Bohemian massif – Evidence from high-pressure metamorphic rocks. *Geologische Rundschau*, *82*(3), 531–555. https://doi.org/10.1007/BF00212415

O'Brien, P. J., & Rötzler, J. (2003). High-pressure granulites: Formation, recovery of peak conditions and implications for tectonics. *Journal of Metamorphic Geology*, *21*(1), 3–20. https://doi.org/10.1046/j.1525-1314.2003.00420.x

Obata, M., Hirajima, T., & Svojtka, M. (2006). Origin of eclogite and garnet pyroxenite from the Moldanubian Zone of the Bohemian Massif, Czech Republic and its implication to other mafic layers embedded in orogenic peridotites. *Mineralogy and Petrology*, *88*(1–2), 321–340. https://doi.org/10.1007/s00710-006-0158-0

Prouteau, G., Scaillet, B., & Pichavant, M. (2001). Hydrous silicic melts derived from subducted oceanic crust. *Nature*, *410*, 197–200.

Rampone, E., & Morten, L. (2001). Records of crustal metasomatism in the garnet peridotites of the ulten zone (Upper Austroalpine, Eastern Alps). *Journal of Petrology*, *42*(1), 207–219. https://doi.org/10.1093/petrology/42.1.207

Rapp, R. P., Watson, E. B., & Miller, C. F. (1991). Partial melting of amphibolite/eclogite and the origin of Archean trondhjemites and tonalites. *Precambrian Research*, *51*(1–4), 1–25. https://doi.org/10.1016/0301-9268(91)90092-O

Reinhardt, J., & Kleemann, U. (1994). Extensional unroofing of granulitic lower crust and related low-pressure, high-temperature metamorphism in the Saxonian Granulite Massif, Germany. *Tectonophysics*, *238*(1–4), 71–94. https://doi.org/10.1016/0040-1951(94)90050-7

Romer, R. L., & Rötzler, J. (2001). P-T–t evolution of ultrahigh-temperature granulites from the Saxon Granulite Massif, Germany. *Part II: Geochronology. Journal of Petrology*, *42*(11), 2015–2032.

Rötzler, J., Hagen, B., & Hoernes, S. (2008). Geothermometry of the ultrahigh-temperature Saxon granulites revisited. Part I: New

evidence from key mineral assemblages and reaction textures. European *Journal of Mineralogy*, *20*(6), 1097–1115. doi:https://doi.org/10.1127/0935-1221/2008/0020-1857.

Rötzler, J., & Romer, R. L. (2001). P-T-t evolution of ultrahigh-temperature granulites from the Saxon Granulite Massif, Germany. *Part I: Petrology. Journal of Petrology*, *42*(11), 1995–2013.

Rötzler, J., Romer, R. L., Budzinski, H., & Oberhänsli, R. (2004). Ultrahigh-temperature high-pressure granulites from Tirschheim, Saxon Granulite Massif, Germany: P-T-t path and geotectonic implications. *European Journal of Mineralogy*, *16*(6), 917–937. https://doi.org/10.1127/0935-1221/2004/0016-0917

Salvioli-Mariani, E., Mattioli, M., Renzulli, A., & Serri, G. (2002). Silicate melt inclusions in the cumulate minerals of gabbroic nodules from Stromboli Volcano (Aeolian Islands, Italy): Main components of the fluid phase and crystallization temperatures. *Mineralogical Magazine*, *66*(6), 969–984. https://doi.org/10.1180/0026461026660071

Scambelluri, M., Hermann, J., Morten, L., & Rampone, E. (2006). Melt-versus fluid-induced metasomatism in spinel to garnet wedge peridotites (Ulten Zone, Eastern Italian Alps): Clues from trace element and Li abundances. *Contributions to Mineralogy and Petrology*, *151*(4), 372–394. https://doi.org/10.1007/s00410-006-0064-9

Schiano, P., Clocchiatti, R., Boivin, P., & Medard, E. (2004). The nature of melt inclusions inside minerals in an ultramafic cumulate from Adak volcanic center, aleutian arc: Implications for the origin of high-Al basalts. *Chemical Geology*, *203*, 169–179. https://doi.org/10.1016/j.chemgeo.2003.10.001

Schiano, P., Clocchiatti, R., Shimizu, N., Maury, R. C., Jochum, K. P., & Hofmann, A. W. (1995). Hydrous, silica-rich melts in the sub-arc mantle and their relationship with erupted arc lavas. *Nature*, *377*(6550), 595–600. https://doi.org/10.1038/377595a0

Schiano, P., Provost, A., Clocchiatti, R., & Faure, F. (2006). Transcrystalline melt migration and earth's mantle. *Science*, *314*(5801), 970–974. https://doi.org/10.1126/science.1132485

Schmädicke, E., Gose, J., & Will, T. M. (2010). The P-T evolution of ultra high temperature garnet-bearing ultramafic rocks from the Saxonian Granulitgebirge Core Complex, Bohemian Massif. *Journal of Metamorphic Geology*, *28*(5), 489–508. https://doi.org/10.1111/j.1525-1314.2010.00876.x

Schmädicke, E., Okrusch, M., & Schmidt, W. (1992). Eclogite-facies rocks in the Saxonian Erzgebirge, Germany: High pressure metamorphism under contrasting P-T conditions. *Contributions to Mineralogy and Petrology*, *110*, 226–241.

Schulmann, K., Lexa, O., Janoušek, V., Lardeaux, J. M., & Edel, J. B. (2014). Anatomy of a diffuse cryptic suture zone: An example from the Bohemian Massif, European Variscides. *Geology*, *42*(4), 275–278. https://doi.org/10.1130/G35290.1

Scott, J. M., Konrad-Schmolke, M., O'Brien, P. J., & Günter, C. (2013). High-T, low-P formation of rare olivine-bearing symplectites in Variscan eclogite. *Journal of Petrology*, *54*(7), 1375–1398. https://doi.org/10.1093/petrology/egt015

Stöckhert, B., Trepmann, C. A., & Massone, H.-J. (2009). Decrepitated UHP fluid inclusions: About diverse phase assemblages and extreme decompression rates (Erzgebirge, Germany). *Journal of Geosciences (Czech Republic)*, *27*, 673–684. https://doi.org/10.1111/j.1525-1314.2009.00835.x

Sun, S.S., & McDonough, W. F. (1989). Chemical and isotopic systematics of oceanic basalts: Implications for mantle composition and processes. *Geological Society, London, Special Publications*, *42*(1), 313–345. https://doi.org/10.1144/GSL.SP.1989.042.01.19

Svojtka, M., Ackerman, L., Medaris, L. G., Hegner, E., Valley, J. W., Hirajima, T., … Hrstka, T. (2016). Petrological, geochemical and Sr-Nd-O isotopic constraints on the origin of garnet and spinel pyroxenites from the Moldanubian Zone of the Bohemian Massif. *Journal of Petrology*, *57*(5), 897–920. https://doi.org/10.1093/petrology/egw025

Timmerman, M. J. (2008). Palaeozoic magmatism. In T. Mccann (Ed.), *The geology of Central Europe. Volume 1: Precambrian and Paleozoic*. London, UK: Geological Society.

Tiraboschi, C., Tumiati, S., Sverjensky, D., Pettke, T., Ulmer, P., & Poli, S. (2018). Experimental determination of magnesia and silica solubilities in graphite-saturated and redox-buffered high-pressure COH fluids in equilibrium with forsterite + enstatite and magnesite + enstatite. *Contributions to Mineralogy and Petrology*, *173*(1), 1–17. https://doi.org/10.1007/s00410-017-1427-0

Veksler, I. V., Nielsen, T. F. D., & Sokolov, S. V. (1998). Mineralogy of crystallized melt inclusions from Gardiner and Kovdor ultramafic alkaline complexes: Implications for carbonatite. *Genesis*, *39*(11–12), 2015–2031.

von Quadt, A. (1993). The Saxonian Granulite Massif: New aspects from geochronological studies. *Geologische Rundschau*, *82*(3), 516–530. https://doi.org/10.1007/BF00212414

von Raumer, J. F., Finger, F., Veselá, P., & Stampfli, G. M. (2014). Durbachites-Vaugnerites – A geodynamic marker in the central European Variscan orogen. *Terra Nova*, *26*(2), 85–95. https://doi.org/10.1111/ter.12071

Vrijmoed, J. C., Austrheim, H., John, T., Hin, R. C., Corfu, F., & Davies, G. R. (2013). Metasomatism in the Ultrahigh-pressure Svartberget Garnet-peridotite (Western Gneiss Region, Norway): Implications for the transport of crust-derived fluids within the mantle. *Journal of Petrology*, *54*(9), 1815–1848. https://doi.org/10.1093/petrology/egt032

Weiss, C. S. (1803). Ueber die Gebirgsart des Sächsischen Erzgebirges welche unter dem Namen Weiss-Stein neuerlich bekannt gemacht worden ist. *Neue Schriften Gesellschaft Naturforschender Freunde*, *4*, 342–366.

Werner, C. D. (1987). Saxonian granulites: A contribution to the geochemical diagnosis of the original rocks in high-metamorphic complexes. *Gerlands Beiträge Zur Geophysik*, *96*, 271–290.

Workman, R. K., & Hart, S. R. (2005). Major and trace element composition of the depleted MORB mantle (DMM). *Earth and Planetary Science Letters*, *231*(1–2), 53–72. https://doi.org/10.1016/j.epsl.2004.12.005

Zanetti, A., Mazzucchelli, M., Rivalenti, G., & Vannucci, R. (1999). The Finero phlogopite-peridotite massif: An example of subduction-related metasomatism. *Contributions to Mineralogy and Petrology*, *134*(2–3), 107–122. https://doi.org/10.1007/s004100050472

Zhang, R. Y., Li, T., Rumble, D., Yui, T.-F., Li, L., Yang, J. S., … Liou, J. G. (2007). Multiple metasomatism in Sulu ultrahigh-P garnet peridotite constrained by petrological and geochemical investigations. *Journal of Metamorphic Geology*, *25*(2), 149–164. https://doi.org/10.1111/j.1525-1314.2006.00683.x

Zhang, Z. M., Dong, X., Liou, J. G., Liu, F., Wang, W., & Yui, F. (2011). Metasomatism of garnet peridotite from Jiangzhuang, southern Sulu UHP belt: constraints on the interactions between crust and mantle rocks during subduction of continental lithosphere. *Journal of Metamorphic Geology*, *29*, 917–937. doi:https://doi.org/10.1111/j.1525-1314.2011.00947.x.

SUPPORTING INFORMATION

Additional supporting information may be found online in the Supporting Information section.

Figure S1. Compositional map of a garnet containing melt inclusions (red ellipse on the bottom right of the figure) of a sample from Rubinberg.

Table S1. Major and trace element composition of the eclogite whole rock from Rubinberg and Klatschmühle.

Table S2. Major and trace element composition with the detection limits of garnet from Rubinberg and Klatschmühle. The garnet analysed for the trace element are not the same minerals as the ones analysed for the major element.

Table S3. Major and trace element composition with the detection limit of clinopyroxenes from Rubinberg and Klatschmühle. The clinopyroxenes analysed for the trace element are not the same minerals as the ones analysed for the major element.

Table S4. Major element composition of plagioclase, biotite and amphibole.

Table S5. Trace element compositions with the detection limits of the melt inclusions.